LETTER **Communicated by S. Coombes**

On Rhythms in Neuronal Networks with Recurrent Excitation

Christoph Börgers
cborgers@tufts.edu
R. Melody Takeuchi
TakeuchiR@wit.edu
Daniel T. Rosebrock
danielr@broadinstitute.org
Department of Mathematics, Tufts University, Medford, MA 02155, U.S.A.

We investigate rhythms in networks of neurons with recurrent excitation, that is, with excitatory cells exciting each other. Recurrent excitation can sustain activity even when the cells in the network are driven below threshold, too weak to fire on their own. This sort of "reverberating" activity is often thought to be the basis of working memory. Recurrent excitation can also lead to "runaway" transitions, sudden transitions to high-frequency firing; this may be related to epileptic seizures. Not all fundamental questions about these phenomena have been answered with clarity in the literature. We focus on three questions here: (1) How much recurrent excitation is needed to sustain reverberating activity? How does the answer depend on parameters? (2) Is there a positive minimum frequency of reverberating activity, a positive "onset frequency"? How does it depend on parameters? (3) When do runaway transitions occur? For reduced models, we give mathematical answers to these questions. We also examine computationally to which extent our findings are reflected in the behavior of biophysically more realistic model networks. Our main results can be summarized as follows. (1) Reverberating activity can be fueled by extremely weak slow recurrent excitation, but only by sufficiently strong fast recurrent excitation. (2) The onset of reverberating activity, as recurrent excitation is strengthened or external drive is raised, occurs at a positive frequency. It is faster when the external drive is weaker (and the recurrent excitation stronger). It is slower when the recurrent excitation has a longer decay time constant. (3) Runaway transitions occur only with fast, not with slow, recurrent excitation. We also demonstrate that the relation between reverberating activity fueled by recurrent excitation and runaway transitions can be visualized in an instructive way by a (generalized) cusp catastrophe surface.

R.M.T. is now at Wentworth Institute of Technology, Boston, MA. D.R. is now at the Broad institute of MIT and Harvard University, Cambridge, MA.

Neural Computation **30, 333–377** (2018)
doi:10.1162/NECO_a_01034

1 Introduction

We think about rhythms in networks of neurons with recurrent excitation, that is, with excitatory cells exciting each other. Recurrent excitation can sustain activity even when the cells in the network are driven below threshold, too weak to fire on their own. This sort of "reverberating" activity is thought to be the basis of working memory (see Compte, Brunel, Goldman-Rakic, & Wang, 2000; Li, Daie, Svoboda, & Druckmann, 2016; McCormick, Hasenstaub, Sanchez-Vives, Badoual, & Bal, 2003; and Riley & Constantinidis, 2015; but also Barak & Tsodyks, 2014; and Mongillo, Barak, & Tsodyks, 2008, for alternative viewpoints). Working memory dysfunction is among the principal impairments associated with schizophrenia (Goldman-Rakic, 1994). Furthermore, in schizophrenia, slow (NMDA receptor-mediated) recurrent excitation in the prefrontal cortex is weakened (Coyle, 2012) and the excitability of excitatory cells raised (Eichhammer et al., 2004). (Simplifying, we will always identify "excitability" and "external drive" in this letter, provided that the external drive is below the firing threshold.) For this reason, the parameter dependence of reverberating activity is of medical interest.

We also study runaway transitions—discontinuous transitions from firing at lower but positive frequencies to higher-frequency firing due to recurrent excitation. There is a potential medical connection here as well: runaway transitions are reminiscent of epileptic seizures (McCormick & Contreras, 2001). There have been discussions in the epilepsy literature about the role of AMPA receptor–mediated (i.e., rapidly decaying) versus NMDA receptor–mediated (slowly decaying) excitation in seizures (Rogawski, 2013); one can view this as a discussion of the parameter dependence of runaway transitions.

We ask three questions:

1. How much recurrent excitation is needed to sustain reverberating activity? How does the answer depend on parameters?
2. Is there a positive minimum frequency of reverberating activity, a positive onset frequency? If so, how does it depend on parameters?
3. When do runaway transitions occur?

We focus on synchronized, rhythmic activity here for two reasons. The first is opportunistic: if we assume idealized, perfect synchronization and idealized, all-to-all connectivity, we can replace a whole network by a single cell with an excitatory autapse or—as a caricature model of a network in which excitatory cells receive feedback inhibition when they fire—with an excitatory and an inhibitory autapse. This allows a much easier yet still instructive mathematical analysis. The second reason is that synchronized, rhythmic activity does in fact seem to play an important role in working memory (Alekseichuk, Turi, de Lara, Antal, & Paulus, 2016; Leszczyński, Fell, & Axmacher, 2015; Roux & Uhlhaas, 2014; Yamamoto, Suh, Takeuchi, & Tonegawa, 2014) and epileptic seizures (Mormann & Jefferys, 2013).

We are by no means the first to have the idea of using a single cell with an autapse as a model of a network with recurrent connectivity (see Gómez, Budelli, & Pakdaman, 2001; Seung, Lee, Reis, & Tank, 2000; Wang, 1999; and Xie & Seung, 2000, for instance). When studying a single cell with an autapse, synchrony is built into the modeling a priori. One loses the ability to address the question of whether there is a synchronous (or nearly synchronous) attracting network state. There is a vast literature on this question, for both purely excitatory networks (Gerstner, van Hemmen, & Cowan, 1996; Mirollo & Strogatz, 1990; Peskin, 1975) and networks including inhibitory neurons (for reviews, see, e.g., Buzsáki & Wang, 2012; Tiesinga & Sejnowski, 2009; Whittington, Traub, Kopell, Ermentrout, & Buhl, 2000; and Börgers, 2017). We do report on some simulations of biophysical model networks of excitatory and inhibitory neurons in this letter, and they confirm that the single-cell analysis yields insight that is relevant for larger networks.

Simplifying somewhat, our answers to our three questions are as follows:

1. There is a positive minimum strength of recurrent excitation needed for reverberating activity when recurrent excitation decays rapidly but not when it decays slowly.

   Experimentally, NMDA, not AMPA receptor-mediated excitation has been found to underlie working memory (Wang & Arnsten, 2015; Wang et al., 2013). Therefore our result suggests that rhythmic reverberating activity lost because of weakening (but not complete loss) of recurrent excitation can always be restored by raising the excitability of pyramidal cells (without raising it so much that the cells fire intrinsically).
2. There is a positive onset frequency. As recurrent excitation gets weaker, the external drive at which onset of reverberating activity occurs gets stronger, and the onset frequency decreases. The onset frequency is lower for slowly decaying recurrent excitation than for rapidly decaying recurrent excitation. As mentioned earlier, hypofunction of NMDA receptors and enhanced excitability of pyramidal cells have been observed in the prefrontal cortex of patients with schizophrenia. In addition, some gamma oscillations have been reported to be slower in schizophrenia patients than in healthy individuals (Spencer et al., 2004). This seems in line with our results. However, regardless of whether this rather speculative connection is real, the parameter dependence of the frequency of reverberating activity is of interest.
3. We prove that runaway transitions require, in our models, the interaction of rapidly decaying recurrent excitation with less rapidly decaying feedback inhibition, and external drive that is not too strong.

Again there is a speculative connection to medicine: perampanel (Zwart et al., 2014), an AMPA receptor antagonist, was approved by the U.S. Food and Drug Administration for the treatment of epilepsy in 2012 (Faulkner & Burke, 2013).

The proofs of these results are elementary, but some are not easy, even for the reduced model problems studied here.

2 Models

We begin by listing the various models we use in this letter.

2.1 Population Activity Model with Recurrent Excitation. The simplest model of recurrent excitation is

$$\frac{df}{dt} = -f + I + g_e S(f),$$

where $S(f) = 0$ for $f < 0$, $S(f) = f$ for $f \in [0, 1]$, and $S(f) = 1$ for $f > 1$. The quantity f is a normalized measure of activity of a neuronal network, such as mean firing frequency measured in a suitable unit; we call it "frequency" from here on. The parameter I is a measure of the external drive or excitability of the cells, and $g_e S(f)$, with $g_e \geq 0$, models recurrent excitation. To make the model aesthetically more appealing and perhaps a little more realistic, we replace S by the smooth approximation $G_\epsilon * S$, where G_ϵ is the gaussian density with mean zero and standard deviation ϵ, and $*$ denotes convolution:

$$\frac{df}{dt} = -f + I + g_e G_\epsilon * S(f). \tag{2.1}$$

In this letter, this highly idealized model mostly serves the purpose of motivating our studies of more realistic models.

2.2 Self-Exciting Integrate-and-Fire Neuron. Our next model is a single linear integrate-and-fire (LIF) neuron, an admittedly crude model of a network of synchronously firing cells.[1] The membrane potential v is shifted and scaled to vary between 0 and 1. When v crosses the threshold value 1, an action potential is assumed to occur, which causes a reset of v to 0 and

[1]The "L" in "LIF" is more commonly taken to stand for "leaky," not "linear." We prefer to interpret it as meaning "linear." Many people consider nonlinear, for instance, quadratic, integrate-and-fire neurons, but very few people consider nonleaky integrate-and-fire neurons. Thus, the "L" in "LIF" conveys information if it stands for "linear," not if it stands for "leaky."

triggers transient self-excitation, which models recurrent excitation in a network. The equations are as follows:

$$\frac{dv}{dt} = -\frac{v}{\tau_m} + I + g_e s_e(t) \qquad \text{if } v < 1, \tag{2.2}$$

$$\frac{ds_e}{dt} = -\frac{s_e}{\tau_e} \qquad \text{if } v < 1, \tag{2.3}$$

$$v(t+0) = 0,\ s_e(t+0) = 1 \qquad \text{if } v(t-0) = 1,\ \frac{dv}{dt}(t-0) > 0. \tag{2.4}$$

Here $\tau_m > 0$ denotes the membrane time constant, I represents external drive or excitability, $g_e \geq 0$ is the strength of recurrent excitation, and $\tau_e > 0$ is the decay time constant. The statement of the reset condition in equation 2.4 is slightly unusual. For a reset to be triggered, it is not sufficient for v to reach 1; it must reach 1 with a positive derivative. This convention will make some later arguments a bit smoother. For $g_e = 0$, periodic firing occurs if and only if $I > I_c$ with

$$I_c = \frac{1}{\tau_m}.$$

Although v is a nondimensionalized membrane potential, we think of t as time measured in ms. However, we think of frequencies as measured in Hz, not in ms^{-1}; the relation between frequency f and period T is therefore not $f = 1/T$ but

$$f = \frac{1000}{T}.$$

We will study periodically firing self-exciting LIF neurons. We pointed out in section 1 that this does not necessarily correspond to a stable (attracting) synchronous network state; this issue cannot be analyzed with a single-cell model. However, one might also ask whether the periodic solutions are stable even as solutions of the single-cell model. If a solution (v, s_e) of equations 2.2 to 2.4 is close to the periodic solution at time 0, will it become the periodic solution eventually? Because of the discontinuous reset described by equation 2.4, this amounts to asking whether there will be a reset; once there is one, what happens from then on is independent of the initial condition. However, in a solution that is initially close to the periodic solution, there will in fact be a reset because of the continuous dependence of the solution of a system of ordinary differential equations on initial conditions. Similar comments apply to the models of sections 2.3 and 2.4 because they too assume discontinuous resets of gating variables.

2.3 Self-Exciting, Self-Inhibiting Integrate-and-Fire Neuron. To the model of the preceding section, we add another term to model feedback inhibition:

$$\frac{dv}{dt} = -\frac{v}{\tau_m} + I + g_e s_e(t) - g_i s_i(t) v \qquad \text{if } v < 1, \tag{2.5}$$

$$\frac{ds_e}{dt} = -\frac{s_e}{\tau_e} \qquad \text{if } v < 1, \tag{2.6}$$

$$\frac{ds_i}{dt} = -\frac{s_i}{\tau_i} \qquad \text{if } v < 1, \tag{2.7}$$

$$v(t+0) = 0, s_e(t+0) = 1, s_i(t+0) = 1 \qquad \text{if } v(t-0) = 1, \frac{dv}{dt}(t-0) > 0. \tag{2.8}$$

Here $g_i \geq 0$ represents the strength of feedback inhibition, and $\tau_i > 0$ is its decay time constant. Note that we model the transient inhibitory current with a reversal term, $-v = 0 - v$. The reversal potential is zero. We might similarly model the transient excitatory current by a term of the form $g_e s_e(t)(v_{\text{rev}} - v)$, not just $g_e s_e(t)$, with $v_{\text{rev}} \gg 1$. However, as v varies from 0 to 1, $v_{\text{rev}} - v$ varies by 100% when $v_{\text{rev}} = 0$, but only by 10% when $v_{\text{rev}} = 10$, as might be roughly appropriate for excitatory synapses. This motivates the simplification of dropping the factor $v_{\text{rev}} - v$ for excitatory synapses, but not for inhibitory ones.

2.4 Self-Exciting Theta Neuron. Our fourth model is a theta neuron (Ermentrout & Kopell, 1986) with self-excitation. For brevity, we make little use of this model in this letter, but we do use it to make one important point later on.

Following Ermentrout (2008), we view the theta neuron as a quadratic integrate-and-fire (QIF) neuron, up to a change of coordinates. We write the QIF neuron as follows:

$$\frac{dv}{dt} = -\frac{v}{\tau_m}(1 - v) + I, \tag{2.9}$$

$$v(t+0) = -\infty \text{ if } v(t-0) = \infty. \tag{2.10}$$

As for the LIF neuron, we think of v as nondimensionalized membrane potential, but of t and τ_m as dimensional times, measured in ms. We say that the QIF neuron fires when v reaches ∞ and is reset to $-\infty$. When $I < 1/(4\tau_m)$, equation 2.9 has the two fixed points,

$$v_{\pm}^* = \frac{1}{2} \pm \sqrt{\frac{1}{4} - \tau_m I}.$$

The fixed point v_-^* is stable, and v_+^* is unstable. As I rises above $1/(4\tau_m)$, the two fixed points collide and annihilate each other. For $I > 1/(4\tau_m)$, there are no fixed points. We write

$$I_c = \frac{1}{4\tau_m}$$

for the QIF neuron.

At first sight, it seems rather dramatically unrealistic to let the firing threshold be $+\infty$ and the reset voltage $-\infty$. However, for $I > 1/(4\tau_m)$, v rises from 1 to ∞, and from $-\infty$ to 0, in a finite (and typically short) amount of time because of the quadratic nonlinearity on the right-hand side of equation 2.9, so defining the reset and threshold voltages to be $-\infty$ and $+\infty$ is in some sense not very different from taking them to be 0 and 1 (see figure 1 of Börgers & Kopell, 2005, for a picture illustrating this point). We let the firing threshold be $+\infty$ and the reset voltage $-\infty$ because then a simple change of coordinates removes the discontinuous reset altogether (Ermentrout, 2008). We will review the change of coordinates shortly.

We add a simple term representing an excitatory autapse:

$$\frac{dv}{dt} = -\frac{v}{\tau_m}(1 - v) + g_e s_e + I, \tag{2.11}$$

$$\frac{ds_e}{dt} = -\frac{s_e}{\tau_e}, \tag{2.12}$$

$$v(t + 0) = -\infty \text{ and } s_e(t + 0) = 1 \text{ if } v(t - 0) = +\infty. \tag{2.13}$$

As before, $g_e \geq 0$ represents the strength of the excitatory autapse and $\tau_e > 0$ its decay time constant. We call the model given by equations 2.11 to 2.13 the *self-exciting QIF neuron*.

In equation 2.11, we introduce the following change of coordinates (Ermentrout, 2008):

$$v = \frac{1}{2} + \frac{1}{2}\tan\frac{\theta}{2}. \tag{2.14}$$

Note that $\theta = 0$ corresponds to $v = 1/2$ (the value around which the right-hand side of equation 2.9, as a function of v, is even), and $\theta = \pm\pi$ correspond to $v = \pm\infty$. Inserting equation 2.14 into 2.11, we find

$$\frac{1}{4\cos^2\frac{\theta}{2}}\frac{d\theta}{dt} = -\frac{1}{4\tau_m}\left(1 - \tan^2\frac{\theta}{2}\right) + g_e s_e + I$$

$$\Leftrightarrow \frac{d\theta}{dt} = -\frac{1}{\tau_m}\left(\cos^2\frac{\theta}{2} - \sin^2\frac{\theta}{2}\right) + 4(g_e s_e + I)\cos^2\frac{\theta}{2}$$

$$\Leftrightarrow \frac{d\theta}{dt} = -\frac{\cos\theta}{\tau_m} + 2(g_e s_e + I)(1 + \cos\theta). \tag{2.15}$$

Equation 2.15 is supplemented by equation 2.12, which remains unchanged. The reset condition, equation 2.13, becomes

$$\theta(t + 0) = -\pi \text{ and } s_e(t + 0) = 1 \text{ if } \theta(t - 0) = \pi. \tag{2.16}$$

Up to notation, the model defined by equations 2.12, 2.15, and 2.16, which we call the *self-exciting theta neuron*, is the self-exciting QIF neuron defined by equations 2.11 to 2.13. Notice, however, that the reset condition for θ in equation 2.16 plays no role for subsequent calculations, since the right-hand side of equation 2.15 is periodic with period 2π; this reset can therefore be omitted without consequence if we replace equation 2.16 by

$$s_e(t + 0) = 1 \text{ if } \theta(t - 0) = \pi \text{ modulo } 2\pi. \tag{2.17}$$

Although θ, the transformed voltage variable, no longer resets discontinuously, the gating variable s_e still does. This discontinuity could be removed by smoothing, but we will refrain from doing so here (see Takeuchi, 2017, where a self-inhibition term is also added).

2.5 Biophysical Network Models. We will compare our results for the very simple model problems with simulations of networks of excitatory and inhibitory cells (E-cells and I-cells), modeled using the Hodgkin-Huxley formalism. For all details of modeling and notation, see the appendix.

3 How Much Recurrent Excitation Is Needed to Sustain Reverberating Activity?

3.1 Population Activity Model with Recurrent Excitation. For the model of section 2.1, we must first explain what "reverberating activity" should mean. For many values of I and g_e, equation 2.1 has a single stable fixed point. However, for some values of I and g_e, there are three fixed points—two stable ones with an unstable one in between. The area in the (I, g_e)-plane for which there are three fixed points will be called the bistability region. The larger of the two fixed points in the bistability region is the analogue of reverberating activity in this model. The cusp catastrophe surface (Strogatz, 2015) in Figure 1 shows the dependence of the fixed points on I and g_e.

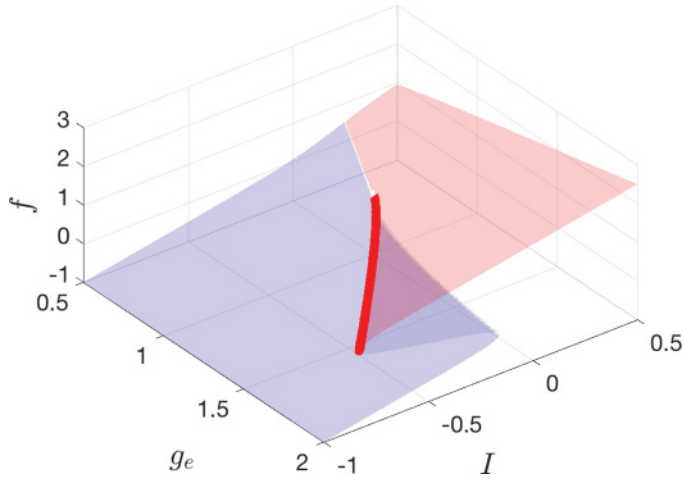

Figure 1: Dependence of the fixed points of equation 2.1 with $\epsilon = 0.2$ on the parameters I and g_e. Unstable fixed points are indicated in gray, stable ones below 1/2 in blue, and stable ones above 1/2 in red. The bold red curve indicates the onset edge of reverberating activity.

Proposition 1. *The region of bistability for equation 2.1 in the (I, g_e)-plane is described by inequalities of the form*

$$g_e > g_0, I_*(g_e) < I < I_c(g_e),$$

where $g_0 > 1$.

So in this simple model, the strength of recurrent excitation needed for the existence of a bistability interval has a strictly positive lower bound.

Proof. The fixed points of equation 2.1 are the f-coordinates of intersection points of the graph of $g_e G_\epsilon * S(f)$ with the graph of $f - I$. A fixed point f_0 is stable if

$$\frac{d}{df}\left(-f + I + g_e G_\epsilon * S(f)\right)\Big|_{f=f_0} < 0,$$

that is,

$$\frac{d}{df}\left(g_e G_\epsilon * S\right)\Big|_{f=f_0} < 1,$$

and unstable if

$$\frac{d}{df}\left(g_e G_\epsilon * S\right)\Big|_{f=f_0} > 1.$$

We note that

$$\frac{d}{df}\left(G_\epsilon * S\right)(f) = \left(G_\epsilon * S'\right)(f), \tag{3.1}$$

where $S'(f)$ denotes the derivative of S. (Note that $S'(f)$ is piecewise constant, defined for $f \neq 0$ and $f \neq 1$. Therefore, $(G_\epsilon * S')(f)$ is defined for all f, and the function $G_\epsilon * S'$ is infinitely often differentiable.) From equation 3.1, it follows immediately that $G_\epsilon * S$ is strictly increasing for all f, and its derivative is strictly increasing for $f \leq 1/2$ and strictly decreasing for $f \geq 1/2$, with a maximal value < 1 at $f = 1/2$. If

$$\frac{d}{df}\left(g_e G_\epsilon * S\right)\Big|_{f=1/2} = g_e\left(G_\epsilon * S'\right)\Big|_{f=1/2} < 1,$$

there is exactly one fixed point, and it is stable. If

$$\frac{d}{df}\left(g_e G_\epsilon * S\right)\Big|_{f=1/2} = g_e\left(G_\epsilon * S'\right)\Big|_{f=1/2} > 1, \tag{3.2}$$

then there is an interval of bistability, a range of values of I of the form

$$I_* < I < I_c$$

for which there are two stable fixed points, one greater than $1/2$ and the other less than $1/2$, with an unstable fixed point in between. We write equation 3.2 in the form $g_e > g_0$, with

$$g_0 = \frac{1}{\left(G_\epsilon * S'\right)\Big|_{f=1/2}} > 1. \tag{3.3}$$

□

3.2 Self-Exciting LIF Neuron. We fix positive values of τ_m and τ_e and plot the firing frequency f of the self-exciting LIF neuron as a function of I and g_e. This results in surfaces of the sort shown in Figure 2, panels A and B, analogous to the cusp catastrophe surface of Figure 1. Note that in panels A and B of Figure 2, the vertical axis denotes $300\tanh(f/300)$, not f. For $f \ll 300$, $300\tanh(f/300) \approx f$, but $300\tanh(f/300)$ cannot exceed 300; this makes the plots easier to read.

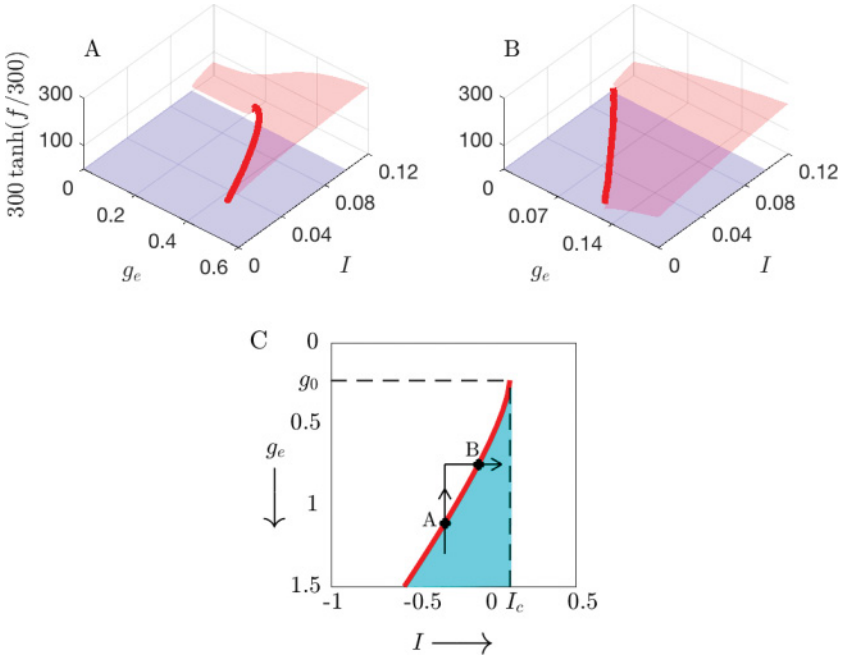

Figure 2: (A) 300tanh($f/300$) as a multivalued function of I and g_e for equations 2.2 to 2.4, with $\tau_m = 10$, $\tau_e = 3$. For all $I \le I_c = 1/\tau_m$ and $g_e \ge 0$, rest is a possibility; this is indicated in blue. For some values of I and g_e ($I > I_c$, but also $I \le I_c$ with g_e large enough), periodic firing is a possibility; this is indicated in red. As before, the onset edge of reverberating activity is drawn as a bold red curve. (Plotting 300tanh($f/300$), not f, makes the figure easier to read.) (B) Same with $\tau_e = 100$. (C) The region in the (I, g_e)-plane in which both rest and periodic firing are possible for the self-exciting LIF neuron, $\tau_m = 10$ and $\tau_e = 3$. Notice that g_e increases in the downward direction here, to make it easier to see how panel C is related to panel A. Along the curve indicated in red, $I = I_*(g_e)$ in the notation of proposition 2. In section 5, we discuss lowering g_e to a point where reverberant activity is lost, then regaining it by raising I—that is, leaving the blue region via point A and reentering it via point B.

Proposition 2. *Let $\tau_m > 0$ and $\tau_e > 0$ be fixed.*

a. The region in the (I, g_e)-plane in which both rest and periodic firing are possible for the self-exciting LIF neuron can be characterized in the form

$$g_e > g_0, I_*(g_e) < I \le I_c, \tag{3.4}$$

where $g_0 \ge 0$ and I_* is a strictly decreasing continuous function of $g_e \ge g_0$ with $I_*(g_0) = I_c$ and $I_*(g_e) \ge I_c - g_e$. See Figure 2C for illustration.

b.

$$g_0 = \max\left(\frac{1}{\tau_e} - \frac{1}{\tau_m}, 0\right). \tag{3.5}$$

Thus, for rapidly decaying recurrent excitation ($\tau_e < \tau_m$), recurrent excitation strength must exceed the positive lower bound $g_0 = 1/\tau_e - 1/\tau_m$ for there to be a range of values $I \leq I_c$ in which there is bistability between rest and reverberating activity. For slowly decaying recurrent excitation ($\tau_e > \tau_m$), there is a range of bistability for any positive g_e. In other words, for slowly decaying recurrent excitation, reverberating activity lost by lowering g_e (keeping it above 0) can always be restored by raising I (keeping it below I_c).

Proof. The proof of this proposition is based on analyzing the initial value problem

$$\frac{dv}{dt} = -\frac{v}{\tau_m} + I + g_e e^{-t/\tau_e}, v(0) = 0, \tag{3.6}$$

which would govern v following an action potential and reset at time 0. The self-exciting LIF neuron fires periodically if and only if the solution v of equation 3.6 rises above 1 at some time.

The solution v of equation 3.6 depends on I and g_e continuously. Furthermore, $v(t)$, $t > 0$ strictly increases with increasing I or g_e. Taken together, these facts imply that the region in the (I, g_e)-plane for which rest is possible ($I \leq I_c$) and periodic firing is possible as well (the solution of equation 3.6 rises above 1 at a finite time) can be characterized in the form of 3.4, with a strictly decreasing function $I_* = I_*(g_e)$.

To prove that I_* is a continuous function of g_e, suppose it were not. Since it is strictly decreasing, any discontinuity would have to be a jump. So suppose that at some value $g_e = \hat{g}_e > g_0$, there were a jump

$$\lim_{g_e \nearrow \hat{g}_e} I_*(g_e) = I_U > I_L = \lim_{g_e \searrow \hat{g}_e} I_*(g_e).$$

By continuity, this would imply that for $g_e = \hat{g}_e$ and $I_L < I < I_U$, the solution v of equation 3.6 would reach, but not exceed, 1 in finite time. This, however, is impossible because for any $t > 0$, $v(t)$ is a strictly increasing function of I. That $I_*(g_0) = I_c$ (i.e., $\lim_{g_e \searrow g_0} I_*(g_e) = I_c$) follows from a very similar argument.

If $I \leq I_c - g_e$, the total drive in the differential equation in equation 3.6, $I + g_e e^{-t/\tau_e}$, remains below I_c for all $t > 0$, and therefore v cannot reach 1. Thus, $I_*(g_e) \geq I_c - g_e$.

This proves part a of the proposition, and all that remains to be proved is the formula for g_0 in equation 3.5. The differential equation in equation 3.6

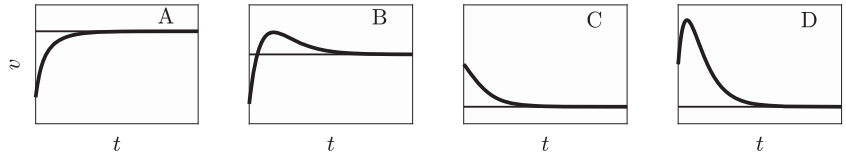

Figure 3: The possible qualitative shapes of solutions of equation 3.6. The horizontal line indicates $\tau_m I$. (A) $I > 0$, $g_e \leq \max(1/\tau_e - 1/\tau_m, 0)\tau_m I$. (B) $I > 0$, $g_e > \max(1/\tau_e - 1/\tau_m, 0)\tau_m I$. (C) $I \leq 0$, $g_e \leq |I|$. (D) $I \leq 0$, $g_e > |I|$.

is scalar and linear with constant coefficients. Therefore, the initial value problem can easily be solved explicitly, using, for instance, an integrating factor. For $\tau_e \neq \tau_m$,

$$v(t) = \tau_m I \left(1 - e^{-t/\tau_m}\right) + g_e \frac{e^{-t/\tau_m} - e^{-t/\tau_e}}{1/\tau_e - 1/\tau_m}. \tag{3.7}$$

Taking the limit as $\tau_e \to \tau_m$, using l'Hospital's rule, we get the solution for the case $\tau_e = \tau_m$:

$$v(t) = \tau_m I \left(1 - e^{-t/\tau_m}\right) + g_e t e^{-t/\tau_m}. \tag{3.8}$$

These formulas imply that $v(t) \to \tau_m I$ as $t \to \infty$.

Some information about the solution can most easily be deduced immediately from the differential equation, without using the explicit formula for the solution. For instance, at a local extremum, $dv/dt = 0$ and therefore $v = \tau_m I + \tau_m g_e e^{-t/\tau_m} > \tau_m I$. Furthermore, differentiating both sides of the differential equation once, we find

$$\frac{d^2 v}{dt^2} = -\frac{1}{\tau_m}\frac{dv}{dt} - \frac{g_e}{\tau_m} e^{-t/\tau_m},$$

which implies that the second derivative is negative at any stationary point—so all stationary points are local maxima. This implies that there are two possible qualitative shapes of the solution v of equation 3.6. Either v converges monotonically to $\tau_m I$ (see Figures 3A and 3C) or v rises initially, reaching a local maximum value greater than $\tau_m I$, and decreasing from then on to the limiting value of $\tau_m I$ (see Figures 3B and 3D). The bumps in Figures 3B and 3D are crucial to our discussion. Similar bumps in voltage traces, for different models but in a similar context, play a central role in Rotstein (2013).

It is not hard to write down the exact condition under which there is a bump. When $I \leq 0$, the condition is

$$\left.\frac{dv}{dt}\right|_{t=0} > 0,$$

that is,

$$g_e > |I|. \tag{3.9}$$

When $I > 0$, there is a bump if and only if $v(t)$ approaches $\tau_m I$ from above. To decide whether $v(t)$ approaches $\tau_m I$ from below or from above, we use the explicit formulas 3.7 and 3.8. If $\tau_e > \tau_m$, we drop the more rapidly decaying exponential e^{-t/τ_m} from the right-hand side of equation 3.7, finding that

$$v(t) \sim \tau_m I + g_e \frac{e^{-t/\tau_e}}{1/\tau_m - 1/\tau_e}$$

for large t, so v approaches $\tau_m I$ from above and there is a bump for any $g_e > 0$. If $\tau_e < \tau_m$, we drop the more rapidly decaying exponential e^{-t/τ_e}, finding

$$v(t) \sim \tau_m I \left(1 - e^{-t/\tau_m}\right) + g_e \frac{e^{-t/\tau_m}}{1/\tau_e - 1/\tau_m},$$

so there is a bump if

$$g_e > \tau_m I \left(\frac{1}{\tau_e} - \frac{1}{\tau_m}\right) \tag{3.10}$$

and no bump if the reverse inequality holds. If the two sides of 3.10 are exactly equal to each other, then equation 3.7 becomes

$$v(t) = \tau_m I - g_e \frac{e^{-t/\tau_e}}{1/\tau_e - 1/\tau_m},$$

so v approaches $\tau_m I$ from below, and therefore there is no bump. The last case we must think about is $\tau_e = \tau_m$. In that case, equation 3.8 is the explicit formula for the solution, and for $g_e > 0$ and large t, clearly $v(t) > \tau_m I$, so there is a bump.

We have now clarified precisely for which parameters each of the four panels of Figure 3 is relevant; the results of our discussion are summarized in the caption of Figure 3. We note that $g_e > g_0$ if and only if the solution v of equation 3.6 with $I = I_c$ exceeds 1 in a finite time, that is, if and only if v has a bump for $I = I_c$. This is the case (see the caption of Figure 3) if and only if

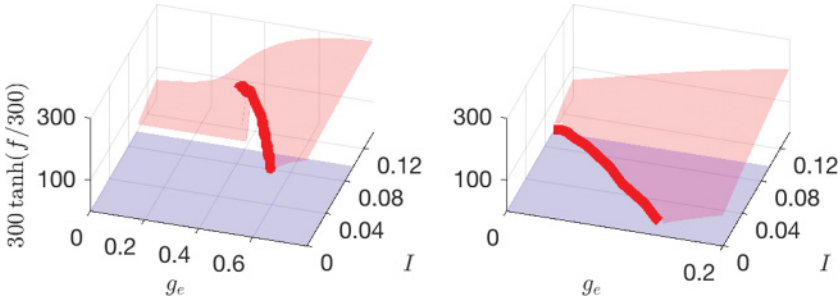

Figure 4: 300tanh($f/300$) as a multivalued function of I and g_e for equations 2.5 to 2.8 with $\tau_m = 10$, $\tau_e = 3$ (left), and $\tau_e = 100$ (right), $g_i = 0.08$, and $\tau_i = 10$. For all $I \le I_c = 1/\tau_m$ and $g_e \ge 0$, rest is a possibility; this is indicated in blue. For some values of I and g_e ($I > I_c$ or $I \le I_c$ but g_e large enough), periodic firing is a possibility as well; this is indicated in red. As before, the onset edge of reverberating activity is drawn as a bold red curve.

$$g_e > \max\left(\frac{1}{\tau_e} - \frac{1}{\tau_m}, 0\right)\tau_m I_c = \max\left(\frac{1}{\tau_e} - \frac{1}{\tau_m}, 0\right).$$

This implies the formula for g_0 given in equation 3.5. □

3.3 Self-Exciting, Self-Inhibiting LIF Neuron. We fix positive values of τ_m, τ_e, g_i, and τ_i and plot the firing frequency f of the self-exciting LIF neuron as a function of I and g_e. This results in surfaces of the sort shown in Figure 4, analogous to the surfaces in Figures 1 and 2. There is an interesting new feature in the left panel of Figure 4: the surface has a tear, that is, there are values of $I > I_c$ for which the firing frequency is a discontinuous function of g_e. We postpone the analysis of the tear to section 6.

Proposition 3. *Let $\tau_m > 0$, $\tau_e > 0$, $g_i > 0$, and $\tau_i > 0$ be fixed.*

a. The region in the (I, g_e)-plane in which both rest and periodic firing are possible for the self-exciting, self-inhibiting LIF neuron can be characterized in the form

$$g_e > g_0, \quad I_*(g_e) < I \le I_c \tag{3.11}$$

for some $g_0 \ge 0$, where I_* is a strictly decreasing continuous function of $g_e \ge g_0$ with $I_*(g_0) = I_c$ and $I_*(g_e) \ge I_c - g_e$. (For illustration, compare Figure 2C.)

b.

$$g_0 \ge \max\left(\frac{1}{\tau_e} - \frac{1}{\tau_m}, 0\right), \tag{3.12}$$

$$g_0 \geq g_i > 0 \ \textit{if} \ \tau_e < \tau_i, \tag{3.13}$$

$$g_0 = 0 \ \textit{if} \ \tau_e > \tau_i \ \textit{and} \ \tau_e > \tau_m. \tag{3.14}$$

Proof. The proof of this proposition is based on analyzing the initial value problem

$$\frac{dv}{dt} = -\frac{v}{\tau_m} + I + g_e e^{-t/\tau_e} - g_i e^{-t/\tau_i} v, \ v(0) = 0, \tag{3.15}$$

which would govern v following an action potential and reset at time 0. The differential equation is almost as simple as that in equation 3.6, scalar and linear, the only complication being that now a time-dependent coefficient multiplies v on the right-hand side. The self-exciting, self-inhibiting LIF neuron fires periodically if and only if the solution v of equation 3.15 exceeds 1 at some time. The proof of part a is in essence identical to the proof of part a of proposition 2.

To prove the estimates on g_0, we note that $g_e > g_0$ if and only if the solution of

$$\frac{dv}{dt} = -\frac{v}{\tau_m} + \frac{1}{\tau_m} + g_e e^{-t/\tau_e} - g_i e^{-t/\tau_i} v, \ v(0) = 0 \tag{3.16}$$

rises above 1 at a finite time. (The only difference between equations 3.15 and 3.16 is that I has been set to $I_c = 1/\tau_m$ in equation 3.16.) The inhibitory term $-g_i e^{-t/\tau_i} v$ can only reduce v, and therefore the value of g_0 with inhibition must be at least as big as that without inhibition; therefore, 3.12 follows from the formula for g_0 in proposition 2. Furthermore, suppose the solution v of equation 3.16 crosses $v = 1$ with a positive slope at time $t = T > 0$. Then

$$g_e e^{-T/\tau_e} - g_i e^{-T/\tau_i} > 0,$$

and if $\tau_e \leq \tau_i$, this is impossible unless $g_e > g_i$. This implies equation 3.13. Finally, note that the solution w of

$$\frac{dw}{dt} = -\frac{w}{\tau_m} + \frac{1}{\tau_m} + g_e e^{-t/\tau_e} - g_i e^{-t/\tau_i}, \ w(0) = 0 \tag{3.17}$$

is a lower bound on the solution v of equation 3.16 as long as $v \leq 1$. It is easy to calculate w explicitly, using an integration factor:

$$w(t) = 1 - e^{-t/\tau_m} + g_e \frac{e^{-t/\tau_m} - e^{-t/\tau_e}}{1/\tau_e - 1/\tau_m} - g_i \frac{e^{-t/\tau_m} - e^{-t/\tau_i}}{1/\tau_i - 1/\tau_m}.$$

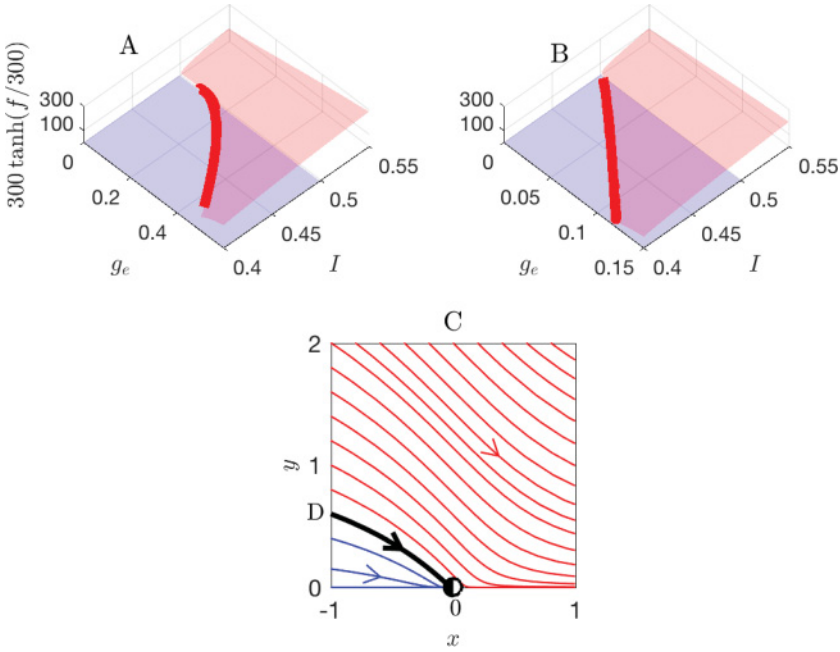

Figure 5: (A) 300tanh($f/300$) as a multivalued function of I and g_e for the self-exciting theta neuron with $\tau_e = 3$, $\tau_m = 1/2$. For all $g_e \geq 0$ and $I \leq I_c = 1/(4\tau_m)$, rest is a possibility; this is indicated in blue. For some values of I and g_e ($I > I_c$ or $I \leq I_c$ but g_e large enough), periodic firing is a possibility; this is indicated in red. (B) Same with $\tau_e = 100$. (C) Phase plane picture for equations 3.23 and 3.24. Trajectories $(x(\tau), y(\tau))$ with $x(\tau) \to \infty$ are indicated in red and trajectories for which $(x(\tau), y(\tau))$ converges to the fixed point in blue. The two regions are bounded by the trajectory indicated in bold black. The borderline trajectory passes through the point $x = -1$, $y = D$, which plays a role in our reasoning.

If τ_e is greater than both τ_m and τ_i, then for large t,

$$w(t) \sim 1 + g_e \frac{e^{-t/\tau_e}}{1/\tau_m - 1/\tau_e} > 1.$$

Thus, w eventually exceeds 1, and therefore so does v. This proves equation 3.14. □

3.4 Self-Exciting Theta Neuron. We fix positive values of τ_m and τ_e and plot the firing frequency f of the self-exciting theta neuron as a function of I and g_e. This results in surfaces of the sort shown in Figures 5A and B, analogous to the surfaces shown previously.

Proposition 4. *Let $\tau_m > 0$ and $\tau_e > 0$ be fixed.*

a. The region in the (I, g_e)-plane in which both rest and periodic firing are possible for the self-exciting theta neuron (see Figure 2C for illustration) can be characterized in the form

$$g_e > g_0, \quad I_*(g_e) < I \leq I_c = \frac{1}{4\tau_m} \tag{3.18}$$

for some $g_0 > 0$, where I_* is a strictly decreasing continuous function of $g_e \geq g_0$ with $I_*(g_0) = I_c$ and $I_*(g_e) \geq I_c - g_e$.

b.

$$g_0 = C\frac{\tau_m}{\tau_e^2} \tag{3.19}$$

for a constant C independent of τ_m and τ_e. Rounded to three significant digits, $C = 1.45$.

Thus, in contrast with the models discussed previously, g_0 is always positive here. However, it is much smaller for large τ_e than for small τ_e.

Proof. The proof of part a is analogous to the proofs of the same statements in the two preceding propositions, except for the claim that g_0 is strictly positive, which will follow from part b.

To prove part b, we write equations 2.11 and 2.12 in terms of nondimensional variables τ, x, and y defined by

$$t = \tau_e \tau, \tag{3.20}$$

$$v = \frac{1}{2} + \frac{\tau_m}{\tau_e} x, \tag{3.21}$$

$$s_e = \frac{\tau_m}{g_e \tau_e^2} y. \tag{3.22}$$

(One is led naturally to these coordinate changes simply by asking which linear coordinate changes result in the maximal simplification of the equations.) With these coordinate changes, equations 2.11 and 2.12 with $I = I_c = 1/(4\tau_m)$ become

$$\frac{dx}{d\tau} = x^2 + y, \tag{3.23}$$

$$\frac{dy}{d\tau} = -y. \tag{3.24}$$

The upper half ($y \geq 0$) of the phase-plane picture for this system is shown in Figure 5C. Because of the quadratic nonlinearity in equation 3.23, trajectories move from $x = -\infty$ to $x = \infty$ (red trajectories) or $x = -1$ (blue

trajectories) in finite time. We omit the elementary arguments proving that indeed the phase-plane picture looks as depicted in Figure 5.

A borderline trajectory, depicted in bold black in Figure 5C, originates at $x = -\infty$, $y = C$ for some finite $C > 0$. To see that C must be finite, suppose that T is the finite time it takes for the borderline trajectory to move from $x = -\infty$ to $x = -1$, and let $D > 0$ be the value of y when the trajectory reaches $x = -1$, (see Figure 5C). Then $C = De^T < \infty$.

It is easy to determine C numerically. Rounding to three significant digits, $C = 1.45$. Trajectories that start at $(x, y) = (-\infty, y_{-\infty})$ reach $x = +\infty$ if and only if $y_{-\infty} > C$. Recalling equations 3.21 and 3.22, we see that this means that starting at $v = -\infty$, the solution of equations 2.11 and 2.12 with $I = I_c = 1/(4\tau_m)$ will reach $+\infty$ if and only if

$$\frac{\tau_e^2}{\tau_m} g_e > C.$$

This implies equation 3.19 and completes the proof. □

3.5 Biophysical Networks. Do our results about the onset of reverberating activity in radically simplified models give any insight into the onset of (rhythmic) reverberating activity in biophysical networks? We refer to the appendix for the definition of our model networks. As explained there, we denote by g_e a measure of the strength of recurrent excitation (g_e is the "$\hat{g}_{ee}$" of the appendix) and by τ_e the decay time constant of recurrent excitation. The decay time constant of E-to-I synapses is always taken to be 3 ms in this letter.

Figures 6A and 6B show two simulations, one with a long (NMDA-like) τ_e and the other with a short (AMPA-like) τ_e. The drive to the E-cells, I, is not far below its threshold value, $I_c \approx 0.12$. In both cases, g_e is chosen so that reverberating activity results, but just barely. As formulas 3.18 and 3.19 would suggest, the threshold value of g_e for reverberating activity is much lower for large τ_e than for small τ_e; this of course is not at all surprising.

As τ_e decreases, g_0 in equation 3.5 is proportional to $1/\tau_e$, while in equation 3.19, it is proportional to $1/\tau_e^2$. In Figures 6A and 6B, the truth seems to be somewhere in between: when τ_e is reduced by about a factor of 33, g_0 rises by about a factor of 147.

The most striking difference between Figures 6A and 6B is of course the difference in the frequency of reverberating activity. This will be discussed in section 4.

Both formulas 3.18 and 3.19 show that the threshold g_0 decreases as the membrane time constant τ_m decreases. Note that for both the LIF and the theta neurons, a reduction in τ_m means an overall acceleration in intrinsic dynamics. When I is near I_c, the intrinsic dynamics bring v to the vicinity of the threshold value 1. This takes less time when τ_m is smaller, and therefore

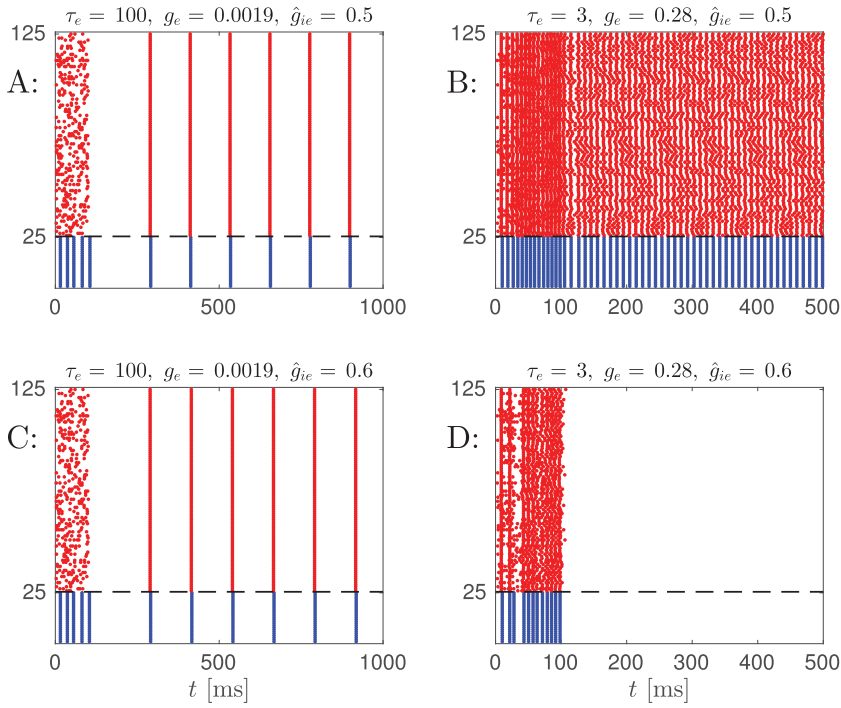

Figure 6: Spike rastergrams for networks of excitatory and inhibitory Hodgkin-Huxley–like cells, modeled as described in the appendix, with parameters $p_{ei} = p_{ie} = p_{ee} = p_{ii} = 1$, $\hat{g}_{ei} = 0.25$, $\hat{g}_{ii} = 0.25$, $I = 0.1$, and τ_e, g_e, and g_{ie} as given in the headings of the panels. All other parameters as defined in the appendix. The vertical axis indicates neuronal indices. Red dots indicate spike times of excitatory cells (E-cells), and blue ones indicate spike times of inhibitory cells (I-cells). The drive $I = 0.1$ is just barely insufficient to sustain firing in the absence of recurrent excitation: $I_c \approx 0.12$ for the E-cells. The values of g_e in panels A and B are chosen to be just barely sufficient to sustain reverberating firing. Panels C and D differ from panels A and B only in the value of g_{ie}, which is slightly raised.

more recurrent excitation will be left at the time v arrives in the vicinity of I_c, making it easier for the recurrent excitation to generate another spike. This reasoning makes the τ_m-dependence in equations 3.18 and 3.19 plausible. However, we have not found any analoge of it in our biophysical networks: greater leakiness of the E-cells does not lead to onset of reverberating activity for lower values of g_e. In fact, a reduction in τ_m in the reduced models is of course not the same as an increase in the leak conductance in the biophysically modeled E-cells; increasing the leak conductance does not amount simply to an overall acceleration of intrinsic dynamics. Further, equations

3.18 and 3.19 are formulas for reverberating activity without feedback inhibition, and in our biophysical networks, feedback inhibition is present and important.

Formula 3.13 suggests that feedback inhibition is crucial in determining whether reverberating activity is possible if the inhibition is slow in comparison with the recurrent excitation. (If it is not, our results in section 3.4 do not say anything about the dependence of g_0 on the strength of feedback inhibition.) Intuitively, this is not hard to understand: Rapidly decaying inhibition will only briefly prevent the recurrent excitation from doing its work, while long-lasting inhibition will block the effect of recurrent excitation long enough for the recurrent excitation to decay substantially and therefore become ineffective. This is confirmed in Figures 6C and D, where the reverberating activity is seen to survive a slight increase in the I-to-E synaptic strength when recurrent excitation decays much more slowly than inhibition, but not when it decays faster than inhibition.

4 Onset Frequency of Reverberating Activity

As noted in section 3, for a fixed $g_e > g_0$, there is a threshold value $I_* = I_*(g_e)$ so that reverberating firing is possible for $I > I_*$ but not for $I \le I_*$ (compare, for instance, Figure 4). We let $f = f(I, g_e)$ be the frequency of reverberating firing for $I > I_*(g_e)$ and call

$$f_*(g_e) = \lim_{I \searrow I_*} f(I, g_e)$$

the "onset frequency of reverberating firing." Since the frequency of reverberating firing is an increasing function of $I > I_*(g_e)$, $f_*(g_e)$ is the infimum of the possible frequencies of reverberating firing for the given g_e.

Alternatively, for a given $I \le I_c$, there is a threshold value $g_{e,*} = g_{e,*}(I)$ so that reverberating firing is possible for $g > g_{e,*}$ but not for $g \le g_{e,*}$. (The function $g_{e,*} = g_{e,*}(I)$ is the inverse of the function $I_* = I_*(g_e)$.) We can think of f_* as a function of I instead of g_e:

$$f_*(I) = \lim_{g_e \searrow g_{e,*}(I)} f(I, g_e).$$

4.1 Self-Exciting, Self-Inhibiting LIF Neuron.

Proposition 5. *For the self-exciting, self-inhibiting LIF neuron, if $I < I_c$,*

$$f_*(I) \ge \frac{1000}{\tau_e \left(1 + \ln\left(1 + \frac{\frac{1}{\tau_e} + g_i}{I_c - I}\right)\right)} > 0. \tag{4.1}$$

Thus, onset of reverberating activity is at positive frequency and at a fast frequency when τ_e is small.

Proof. We must give an upper bound on the time T at which the solution v of the initial value problem 3.15 crosses the threshold value 1. At the time T when v crosses 1,

$$\frac{dv}{dt} = -\frac{1}{\tau_m} + I + g_e e^{-T/\tau_e} - g_i e^{-T/\tau_i} > 0.$$

This implies

$$-\frac{1}{\tau_m} + I + g_e e^{-T/\tau_e} > 0$$

and, thus (using $I_c = 1/\tau_m$),

$$T < \tau_e \ln \frac{g_e}{I_c - I}. \tag{4.2}$$

This shows that T is small if τ_e is short unless g_e is very large.

However, if g_e is very large, then T is small for an even simpler reason: there is, for a brief amount of time, a large amount of recurrent excitation. For instance, for $0 < t \leq \tau_e$, the total (external and synaptic) drive satisfies the inequality

$$I + g_e e^{-t/\tau_e} - g_i e^{-t/\tau_i} > I + \frac{g_e}{e} - g_i.$$

Thus, if the solution w of

$$\frac{dw}{dt} = -\frac{w}{\tau_m} + I + \frac{g_e}{e} - g_i, \;\; w(0) = 0 \tag{4.3}$$

reaches 1 in the time interval $[0, \tau_e]$, then v exceeds 1 in the same interval. The solution of 4.3 can easily be written down explicitly:

$$w(t) = \tau_m \left(I + \frac{g_e}{e} - g_i \right) \left(1 - e^{-t/\tau_m} \right).$$

We conclude

$$\begin{aligned} & T < \tau_e \Leftarrow \\ & \tau_m \left(I + \frac{g_e}{e} - g_i \right) \left(1 - e^{-\tau_e/\tau_m} \right) \geq 1 \Leftarrow \end{aligned} \tag{4.4}$$

$$\tau_m \left(I + \frac{g_e}{e} - g_i\right)\left(1 - \frac{1}{1+\tau_e/\tau_m}\right) \geq 1 \Leftrightarrow \tag{4.5}$$

$$\left(I + \frac{g_e}{e} - g_i\right)\frac{1}{1/\tau_e + I_c} \geq 1 \Leftrightarrow$$

$$g_e \geq \left(I_c - I + \frac{1}{\tau_e} + g_i\right)e. \tag{4.6}$$

Inequality 4.5 implies 4.4 because for all real x,

$$e^x \geq 1 + x, \text{ i.e., } e^{-x} \leq \frac{1}{1+x}.$$

If 4.6 does not hold, that is, if

$$g_e < \left(I_c - I + \frac{1}{\tau_e} + g_i\right)e,$$

then by 4.2,

$$T < \tau_e \ln \frac{\left(I_c - I + \frac{1}{\tau_e} + g_i\right)e}{I_c - I} = \tau_e \left(1 + \ln\left(1 + \frac{\frac{1}{\tau_e} + g_i}{I_c - I}\right)\right). \tag{4.7}$$

But if 4.6 does hold, then $T < \tau_e$, which is smaller than the right-hand side of 4.7. Therefore, in any case, 4.7 holds, and this implies 4.1. □

4.2 Self-Exciting Theta Neuron.

Proposition 6. *For the self-exciting theta neuron, the onset frequency f_* of reverberating activity is zero for all parameter values.*

Our reasoning will not be entirely rigorous here. The onset frequency f_* is zero because in the limit as $g_e \searrow g_{e,*}(I)$, reverberating activity is lost as a result of a saddle-cycle collision. To see this, we rewrite equations 2.11 and 2.12 using the coordinate changes, of equations 3.20 to 3.22 but this time assuming $I < I_c = 1/(4\tau_m)$. (We had previously done this for $I = I_c$, and obtained equations 3.23 and 3.24.) We obtain

$$\frac{dx}{d\tau} = x^2 + y + J, \tag{4.8}$$

$$\frac{dy}{d\tau} = -y, \tag{4.9}$$

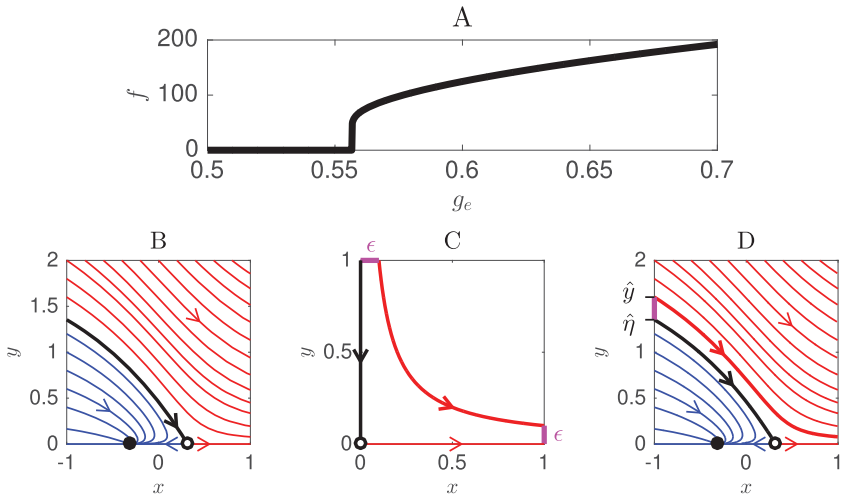

Figure 7: (A) f as a function of g_e for the self-exciting theta neuron with $\tau_m = 1/2$, $\tau_e = 100$, and $I = 0$. The f-g_e-curve is continuous, but steep to infinite order at onset. (B) Phase-plane pictures for equations 4.8 and 4.9 with $J = -0.1$. Trajectories $(x(\tau), y(\tau))$ with $x(\tau) \to \infty$ are indicated in red and trajectories for which $(x(\tau), y(\tau))$ converges to the stable node in blue. (C) Trajectory passing near a saddle point. (D) Same as panel (B) but indicating $\hat{\eta}$ and $\hat{y}$ (see text).

where

$$J = \frac{(I - I_c)\tau_e^2}{\tau_m} < 0.$$

Figure 7B shows the phase-plane picture for $J = -0.1$. Different values $g_e > g_{e,*}(I)$ correspond to different red trajectories in Figure 7B. As $g_e \searrow g_{e,*}(I)$, the trajectory merges with the bold black trajectory in Figure 7B, which follows the stable manifold of the saddle point. As the distance between saddle and cycle becomes infinitesimally small, so does the speed of motion in the vicinity of the saddle. As a result, the frequency becomes infinitesimally small.

At first sight, proposition 6 seems to be bad news for us: the inequality proved in section 4.1 seems to be irrelevant for the theta neuron, which is arguably a more realistic neuronal model than the LIF neuron. However, although the frequency, f, of reverberating activity starts out at zero as g_e rises above $g_{e,*}(I)$, the rise in f is extremely rapid (see Figure 7A). We will argue heuristically that the frequency f, as a function of $g_e \geq g_{e,*}$, is not just infinitely steep, but steep to infinite order at $g_{e,*}$. By this statement, we mean

that g_e, as a function of $f \geq 0$, is flat to infinite order, that is, all derivatives of g_e with respect to f are zero at $f = 0$.

This follows from a general observation about flow in the vicinity of a saddle. Suppose that a trajectory passes a saddle point at a small distance $d > 0$. Near the saddle point, the motion must of course be slow, since the saddle is a fixed point, albeit an unstable one. The time T that the passage takes (a notion made completely precise in a simple example below) diverges to ∞ as $d \to 0$. However, this divergence is only logarithmic. Thus, for the passage to take a long time, d must be very close to 0. Consequently, when a limit cycle is broken in a saddle-cycle collision, the oscillation gets slow only when the saddle comes very close to the cycle.

For illustration, consider the model system

$$\frac{dx}{dt} = x, \ \frac{dy}{dt} = -y, \tag{4.10}$$

which has a saddle point at the origin. Let $\epsilon \in (0, 1)$, and suppose at time $t = 0$, the trajectory starts at $(x, y) = (\epsilon, 0)$. The time at which the trajectory arrives at $(x, y) = (1, \epsilon)$ (see Figure 7C) equals $T = \ln(1/\epsilon)$. Solving for ϵ and setting $T = 1000/f$, we find

$$\epsilon = e^{-1000/f}.$$

Thus, the function $\epsilon = \epsilon(f)$ is flat to infinite order at $f = 0$, or f as a function of ϵ is steep to infinite order at $\epsilon = 0$. (Since the distance at which the trajectory passes the saddle at the origin is $d = \sqrt{2\epsilon}$, the same statement holds for f as a function of d.)

To clarify the connection between the model system, equation 4.10, and equations 4.8, 4.9, note that the bold curve in Figure 7B is the stable manifold of the saddle point, the analoge of the y-axis in Figure 7C. Denote this curve by $(\xi(\tau), \eta(\tau))$, with $\xi(0 + 0) = -\infty$ and $\eta(0 + 0) = \eta_* > 0$. Let $(x(\tau), y(\tau))$ be one of the red curves in Figure 7B and assume $x(0 + 0) = -\infty$ and $y(0 + 0) = y_*$. The trajectory (ξ, η) enters the strip $[-1, 1] \times \mathbb{R}$ at a point $(-1, \hat{\eta})$, and the trajectory (x, y) enters it at a point $(-1, \hat{y})$ with $\hat{y} > \hat{\eta}$ (see Figure 7D). The difference $\hat{y} - \hat{\eta}$ is the analog of the ϵ of Figure 7C. Because η and x move from $-\infty$ to -1 in finite time, $\hat{y} - \hat{\eta}$ and $y_* - \eta_*$ are proportional to each other in the limit as $y_* \searrow \eta_*$. (Numerical experiments confirm that this is true with considerable accuracy even for values of $y_* - \eta_*$ and $\hat{y} - \hat{\eta}$ that are not extremely small.) Finally, the difference $y_* - \eta_*$ is proportional to $g_e - g_{e,*}$.

Although we have discussed the f-g_e curve with a fixed I here, a similar conclusion holds, for similar reasons, for the f-I curve with a fixed g_e. It is steep to infinite order at $I = I_*(g_e)$ because there is a saddle-cycle collision in the limit $I \searrow I_*(g_e)$ (see also section 17.3 of Börgers, 2017).

4.3 Biophysical Networks. Our analysis of model problems suggests that slow, rhythmic reverberating activity might be possible when τ_e is large but not when it is short. This much is not surprising. It is the reason why synchrony has been suggested as a way of terminating reverberating activity driven by rapidly decaying recurrent excitation (Gutkin, Laing, Colby, Chow, & Ermentrout, 2001).

Inequality 4.1 suggests a second, more subtle conclusion, however. For large τ_e, the lower bound in 4.1 is about $1000/\tau_e$. For small τ_e, it is substantially smaller than $1000/\tau_e$. Although the expression in equation 4.1 is just a lower bound on $f_*(I)$, not an exact expression for $f_*(I)$, the simulations in Figures 6A and 6B are in agreement with this observation: for $\tau_e = 100$ (see Figure 6A) the lowest frequency of reverberating activity that we were able to generate, by choosing g_e very carefully just barely greater than needed to see any reverberating activity activity, is just a little bit smaller than $1000/\tau_e = 10$ Hz. For $\tau_e = 3$ (see Figure 6B), the slowest possible reverberating activity is at a high frequency, but the frequency is just slightly above 100 Hz, nowhere near $1000/\tau_e \approx 333$ Hz.

We believe that for the biophysical networks, the onset frequency, at least for perfectly synchronous E- and I-cell populations without any heterogeneity, is in fact zero, as it is for the self-exciting theta neuron. However, very low frequencies are possible only in a parameter regime so narrow that it may be of no practical consequence (compare Figure 7A).

5 Frequency Shift Resulting from Compensating for Weak Recurrent Excitation with Excitability

In the surfaces in Figures 1, 2, and 4, there is an onset edge of reverberating activity, indicated in bold red in the figures. In each case, the frequency f_* along the onset edge is nonzero and an increasing function of g_e. This sounds completely unsurprising—stronger recurrent excitation yields faster firing. However, notice that along the onset edge, the direction of increasing g_e is the direction of decreasing I—less excitability (lower I) produces faster onset. This, of course, sounds more surprising.

For the self-exciting and self-inhibiting LIF neuron, it is elementary but not at all easy to prove that f_* is an increasing function of g_e, that is, a decreasing function of I. For brevity, we omit this proof here. In section 5.1, we merely give the very straightforward proof for the population activity model (i.e., for Figure 1). For the self-exciting theta neuron, the onset frequency is zero (see proposition 6). However, we demonstrate numerically in section 5.2 that $f(1.01I_*(g_e), g_e)$ is still an increasing function of g_e. Thus, if I is chosen just 1 percent greater than $I_*(g_e)$, the behavior is as for the other single-cell models.

The monotonicity of f along the onset edge is interesting for the following reason. Suppose that g_e is weakened beyond the point where reverberating activity is lost and then restored by raising "excitability," that is,

raising I. The reverberating activity then re-appears at a lower frequency than that at which it was lost. Figure 2C illustrates this point. Leaving the region of reverberating activity by lowering g_e, then reentering it by raising I, involves a downward frequency shift: f_* is lower in Figure 2B than in 2A.

As discussed in section 1, in schizophrenia, both NMDA receptor hypofunction and increased excitability of pyramidal cells have been reported, and so have downward shifts in oscillation frequencies. Our analysis here may or may not be related to these observations, but in any case, it shows an interesting case in which compensation for parameter abnormalities leads to a shift in oscillation frequencies.

5.1 Population Activity Model.

Proposition 7. *For the population activity model of section 3.1, let $f_* = f_*(g_e)$ denote the larger of the two fixed points at the onset edge of reverberating activity, $I = I_*(g_e)$. Then f_* is a strictly increasing function of g_e.*

Proof. From the discussion in the proof of proposition 1, we see that f_* is characterized by the conditions $f_* \geq 1/2$ and

$$\frac{d}{df}\,(g_e G_\epsilon * S)\bigg|_{f=f_*} = 1,$$

that is,

$$\frac{d}{df}\,(G_\epsilon * S)\bigg|_{f=f_*} = \frac{1}{g_e}. \tag{5.1}$$

Since $\frac{d}{df}\,(G_\epsilon * S)$ is a decreasing function of $f \geq 1/2$, equation 5.1 implies that f_* is an increasing function of g_e. □

5.2 Self-Exciting Theta Neuron. For the self-exciting theta neuron, there is no precise analog of the downward frequency shift discussed above, since the onset frequency of reverberating activity is zero. However, if we replace the definition of the onset frequency by

$$f_*(g_e) = f(1.01 I_*(g_e), g_e) \tag{5.2}$$

(the factor of 1.01 is, of course, somewhat arbitrary), then the onset frequency is positive (and not small), and empirically it is a strictly increasing function of g_e, as Figure 8 shows.

5.3 Biophysical Networks. Our main point in section 5 has been that there will be a downward frequency shift when reverberating activity is lost by weakening recurrent excitation, then restored by raising excitability.

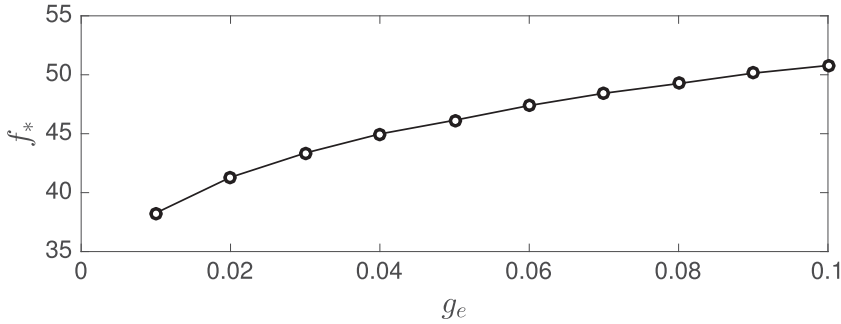

Figure 8: The modified $f_*(g_e)$, defined as in equation 5.2, as a function of g_e, for the self-exciting theta neuron with $\tau_m = 1/2$, $\tau_e = 100$.

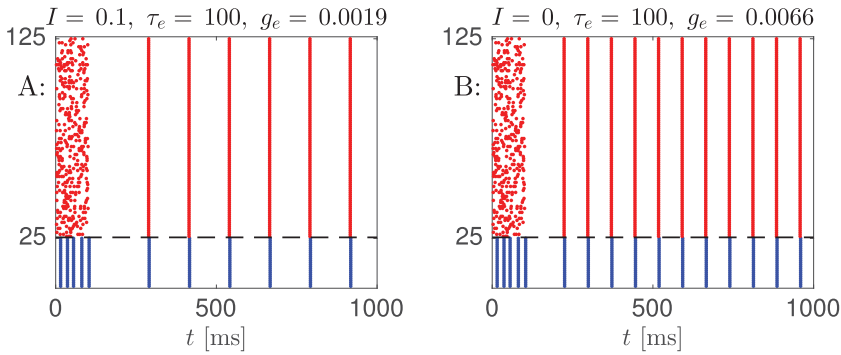

Figure 9: (A) Same as Figure 6C. (B) Same except for a reduction in I and an increase in g_e, as indicated in the heading of the panel. In both panels, the value of g_e is just barely sufficient to sustain reverberating activity: if the last significant digit were reduced by 1, there would be no reverberating activity.

Figure 9 illustrates this in network simulations. In both panels of the figure, g_e is chosen just barely above $g_{e,*}(I)$.

6 Runaway Transitions

We will prove in section 6.1 that for the self-exciting, self-inhibiting LIF neuron, discontinuous transitions from firing at lower (but positive) frequencies to higher-frequency firing requires the interaction of rapidly decaying recurrent excitation with less rapidly decaying feedback inhibition, and external drive that is not too strong. Then, in section 6.2, we demonstrate similar principles in biophysical network simulations.

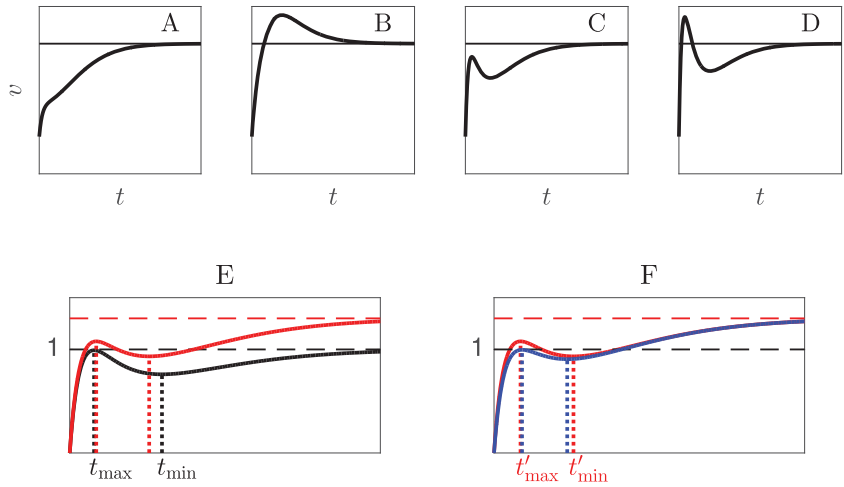

Figure 10: (A–D) Possible qualitative shapes of solutions $v = v(t)$ of equation 3.15 for $I > 0$. The horizontal line indicates the limiting value $v = \tau_m I$. E, black: Solution of equation 3.15 when $I = I_c, g_e = g_{e,*}$ chosen so that $f(I_c, g_e)$ has a jump discontinuity at $g_{e,*}$. (E, F red) Solution of equation 3.15 with $g_e = g_{e,ast}, I = \hat{I} > I_c$. (F, blue) Solution of equation 3.15 with $I = \hat{I}$, but with g_e lowered so that the local maximum value drops back to 1.

6.1 Self-Exciting, Self-Inhibiting LIF Neuron. We will analyze under which circumstances the frequency of the self-exciting, self-inhibiting LIF neuron depends discontinuously on g_e, for fixed $I > I_c$. Our discussion is based on a detailed analysis of the initial value problem, equation 3.15. First, we describe the possible qualitative shapes of the solutions of that problem.

Lemma 1. *Let $I > 0$, $\tau_m > 0$, $g_e > 0$, $\tau_e > 0$, $g_i > 0$, $\tau_i > 0$. Let $v = v(t)$ be the solution of equation 3.15. Then the graph of v looks qualitatively like one of panels A to D of Figure 10. That is, $dv/dt > 0$ at $t = 0$, and v has zero, one, or two local extrema. Two local extrema, as in panels C and D, are possible only if $\tau_e < \tau_i$.*

Proof. The function dv/dt is nonconstant and analytic in the mathematical sense: it is locally represented by its Taylor series. Its zeros therefore cannot have an accumulation point, and the local extrema of v can be ordered in the form

$$0 < t_1 < t_2 < \dots$$

In between local extrema, v is strictly monotonic. At time $t = 0$,

$$\frac{dv}{dt} = I + g_e > 0,$$

and therefore t_1 is a local maximum, t_2 a local minimum, and so on. This implies

$$v(t_k) > v(t_{k+1}) \quad \text{if } k \text{ is odd,} \tag{6.1}$$

$$v(t_k) < v(t_{k+1}) \quad \text{if } k \text{ is even.} \tag{6.2}$$

Let us consider the second derivative of v in an extremum t_k, $k = 1, 2, \ldots$:

$$\begin{aligned}\frac{d^2v}{dt^2}(t_k) &= \frac{d}{dt}\left(-\frac{v}{\tau_m} + I + g_e e^{-t/\tau_e} - g_i e^{-t/\tau_i} v\right)\Big|_{t=t_k} \\ &= -\frac{g_e}{\tau_e} e^{-t_k/\tau_e} + \frac{g_i}{\tau_i} e^{-t_k/\tau_i} v(t_k). \end{aligned} \tag{6.3}$$

(We used here that $dv/dt = 0$ at a local extremum.) If k is odd, then t_k is a local maximum, therefore, equation 6.3 must be ≤ 0, so

$$v(t_k) \leq Q(t_k) \quad \text{if } k \text{ is odd,} \tag{6.4}$$

with

$$Q(t) = \frac{g_e \tau_i}{g_i \tau_e} e^{-t/\tau_e + t/\tau_i}.$$

Similarly,

$$v(t_k) \geq Q(t_k) \quad \text{if } k \text{ is even.} \tag{6.5}$$

If $\tau_e < \tau_i$, Q is strictly decreasing and

$$v(t_2) \geq Q(t_2) > Q(t_3) \geq v(t_3).$$

The first inequality follows from 6.5, the second from the fact that Q is strictly decreasing, and the third from 6.4. But now we conclude $v(t_2) > v(t_3)$, which contradicts 6.2. The only way out is that there is no "t_3"—there are at most two local extrema, and therefore, panels Figures 10A to 10D are the only possibilities. If $\tau_e \geq \tau_i$, then Q is increasing, and

$$v(t_1) \leq Q(t_1) \leq Q(t_2) \leq v(t_2).$$

The first inequality follows from 6.4, the second from the fact that Q is increasing, and the third from 6.5. But now we conclude $v(t_1) \leq v(t_2)$, which contradicts 6.1. The only possible conclusion is that there is no "t_2"; there is at most one local extremum, and therefore, panels A and B of Figure 10 are now the only possibilities. □

Lemma 2. *If $f(I_c, g_e)$, as a function of g_e, has a jump discontinuity, then so does $f(I, g_e)$ for $I > I_c$ sufficiently close to I_c.*

Proof. We use the fact that solutions of equations 3.15 with $I > 0$ must have one of the shapes shown in panels A to D of Figure 10. If $f(I_c, g_e)$, as a function of g_e, has a jump discontinuity at $g_{e,*} \geq 0$, then the graph of v as a function of t, for $I = I_c$ and $g_e = g_{e,*}$, must have the shape shown in panels C and D of Figure 10, with a local maximum value $= 1$ reached at some time $t_{\max} > 0$, followed by a local minimum value < 1 reached at some time $t_{\min} > t_{\max}$ (see the black curve in Figure 10E).

Suppose now that we fix $g_e = g_{e,*}$ and raise I to a new value $\hat{I} > I_c$. The solution, v, of equation 3.15 is a strictly increasing continuous function of I. If $\hat{I}$ is not too large, there must still be a local minimum value < 1, but the local maximum value is now greater than 1 (see the red curve in Figure 10E, reproduced in Figure 10F). The times at which the local maximum and the local minimum occur for $I = \hat{I}$ and $g_e = g_{e,*}$ are not the same as $t_{\max}$ and $t_{\min}$; we denote them by $t'_{\max}$ and $t'_{\min}$.

Now suppose that we fix I at $\hat{I}$ and lower g_e. Since the solution of equation 3.15 is also a strictly increasing continuous function of g_e, the maximum of $v(t)$ over the interval $[0, t'_{\min}]$ continuously decreases. At some value $g_e = \hat{g}_e$, this maximum becomes equal to 1 (see the blue curve in Figure 10F). The function $f(\hat{I}, g_e)$ is discontinuous at $g_e = \hat{g}_e$. □

Proposition 8. *(a) In the self-exciting, self-inhibiting LIF neuron, there is a runaway transition, that is, a jump discontinuity in the frequency f as a function of g_e for some fixed value of $I > I_c$, if and only if $\tau_e < \tau_i$. (b) A runaway transition can occur only if $I < I_c + g_i$.*

Proof. Let $I = \hat{I} > I_c$ and $g_e \geq 0$. The self-exciting, self-inhibiting LIF neuron fires periodically since $I > I_c$. Let T be the period of firing. Recalling that we say that the LIF neuron fires only when v rises strictly above the threshold 1, we see that T is characterized by $v(t) \leq 1$ for $t \leq T$, and $v(t) > 1$ for $t > T$, $t - T$ small enough, where v denotes the solution of equation 3.15. If $v(t) < 1$ for $t \in [0, T)$, then T depends continuously on g_e because of the continuous dependence of solutions of ordinary differential equations on parameters on the right-hand side. However, if $v(t_{\max}) = 1$ for some $t_{\max} \in [0, T)$, then T depends discontinuously on g_e: an infinitesimal increase in g_e makes T drop discontinuously to $t_{\max}$.

If $f(\hat{I}, g_e)$ is a discontinuous function of g_e and if the discontinuity occurs at $g_e = \hat{g}_e$, then the solution of equation 3.15 with $I = \hat{I}$ and $g_e = \hat{g}_e$ must have the shape shown in Figures 10C and 10D (with a local maximum value of 1), and therefore $\tau_e < \tau_i$ by lemma 1. At the time $t_{\max}$ at which v has its local maximum, $v = 1$ and $dv/dt = 0$, so

$$-\frac{1}{\tau_m} + I + g_e e^{-t_{\max}/\tau_e} - g_i e^{-t_{\max}/\tau_i} = 0.$$

Solving for I, we find

$$I = \frac{1}{\tau_m} + g_i e^{-t_{\max}/\tau_i} - g_e e^{-t_{\max}/\tau_e} < \frac{1}{\tau_m} + g_i = I_c + g_i.$$

This proves most of proposition 6.1 already.

What remains to be shown is that f, as a function of g_e, does indeed have a discontinuity for some $I = \hat{I} > I_c$ when $\tau_e < \tau_i$. So assume now that $\tau_e < \tau_i$. We will prove that $f(I_c, g_e)$, as a function of g_e, has a jump discontinuity. By lemma 2, this implies that $f(I, g_e)$, as a function of g_e, has a jump discontinuity for $I > I_c$, $I - I_c$ small enough.

If $g_e = 0$, then $f(I_c, g_e) = 0$. For sufficiently large, positive g_e, $f(I_c, g_e) > 0$. Furthermore, $f(I_c, g_e)$ is monotonically increasing as a function of g_e. There is therefore some $g_{e,*} \geq 0$ so that $f(I_c, g_e) = 0$ for $g_e < g_{e,*}$, and $f(I_c, g_e) > 0$ for $g_e > g_{e,*}$.

We note that $g_e \leq g_i$ implies $f(I_c, g_e) = 0$. To see this, consider the right-hand side of the differential equation in equation 3.15 at $v = 1$, using that $I = I_c = 1/\tau_m$:

$$\left.\frac{dv}{dt}\right|_{v=1} = g_e e^{-t/\tau_e} - g_i e^{-t/\tau_i}.$$

If $g_e \leq g_i$ and $\tau_e < \tau_i$, this is negative for $t > 0$, so $v(t)$ cannot cross the value $v = 1$. Thus $g_{e,*} \geq g_i$ (compare 3.13).

If v crosses the threshold 1 at time T, then

$$\left.\frac{dv}{dt}\right|_{t=T} = g_e e^{-T/\tau_e} - g_i e^{-T/\tau_i} > 0.$$

Solving for T and using that $\tau_e < \tau_i$, we find

$$T < \frac{\ln(g_e/g_i)}{1/\tau_e - 1/\tau_i}$$

or

$$f \geq 1000 \frac{1/\tau_e - 1/\tau_i}{\ln(g_e/g_i)}.$$

This implies

$$\lim_{g_e \searrow g_{e,*}} f(I_c, g_e) \geq 1000 \frac{1/\tau_e - 1/\tau_i}{\ln(g_{e,*}/g_i)} > 0, \tag{6.6}$$

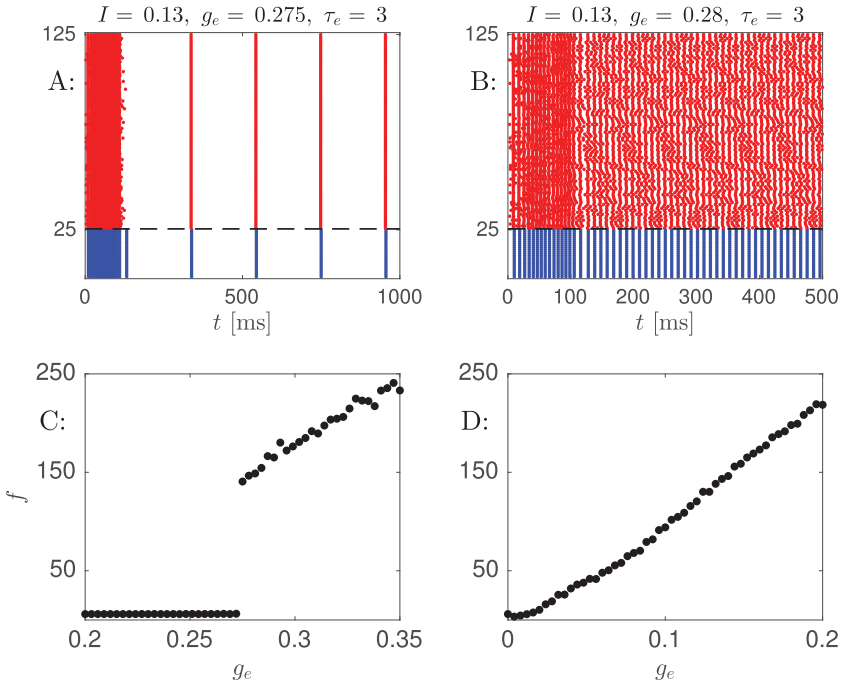

Figure 11: (A, B) Stepping across the "tear" in the f-I-g_e surface for the E-I network. Parameters as in Figure 6B, except for the parameters specified in the titles of the panels. The external drive I is now slightly above threshold, and recurrent excitation decays fast. (C) Results of network simulations with parameters as in panels A and B, except for g_e, which is varied here. The plot shows the mean frequency of the E-cells in the last 500 ms of simulated time, as a function of g_e. (D) Same as panel C, except that now the decay time constant of recurrent excitation is 20 ms.

so $f(I_c, g_e)$ has a jump discontinuity at $g_e = g_{e,*}$. Incidentally, it also implies that $g_{e,*}$ is strictly greater than g_i, since otherwise 6.6 would imply $\lim_{g_e \searrow g_{e,*}} f(I_c, g_e) = \infty$. □

6.2 Biophysical Networks. Figures 11A and 11B show a "runaway transition" in the sense in which we use the phrase: a discontinuous change from slow (but positive) to fast firing frequencies as recurrent excitation strength is raised. One can easily find such transitions for rapidly decaying (AMPA-like) recurrent excitation, as in Figures 11A and 11B.

The abrupt transition from low-frequency firing to high-frequency firing is illustrated again in Figure 11C, which shows the mean frequency f of the E-cells as a function of g_e for $I = 0.13$. Proposition 6.1 suggests that the tear

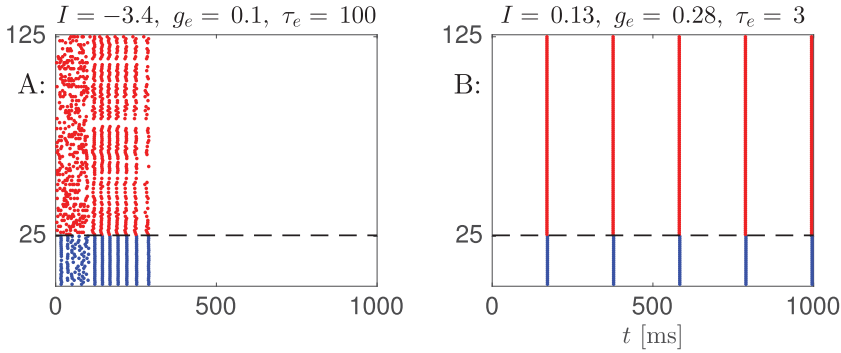

Figure 12: Phenomena in networks that cannot be reproduced in the single-cell models. (A) Parameters as in Figure 6A, except for those given in the titles of the panels and with 20% of all synaptic connections removed and the others strengthened by a factor of 1.25: $p_{ei} = p_{ie} = p_{ee} = p_{ii} = 0.80$. The network comes to rest after multiple spike volleys. (B) Same as Figure 11B but with synchronous initialization. Low- and fast-frequency activity are possible with the same parameters.

should arise only if τ_e is sufficiently small in comparison with τ_i. Figure 11D shows an f-g_e curve similar to that in the upper panel, but with τ_e raised from 3 ms to 20 ms. Indeed the discontinuity has disappeared.

7 Two Network Effects Not Seen in Single-Cell Models

Up to now, our networks have been homogeneous, and that has usually resulted in near-perfect synchronization soon after the initial stochastic stimulation ceases. As stated in section A.5, we take the external drive to the E-cells to be homogeneous, equal to I for all E-cells, so that there is an unambiguous definition of external drive above or below threshold. However, in section 7.1 we introduce heterogeneity by making the synaptic connections sparse and random. This results in less-than-perfect synchronization, suppression of a varying number of E-cells, and, as a result, a "memory" effect not seen in the simpler earlier models. In section 7.2, we show an example of the coexistence of slow, tightly synchronous, and fast, only loosely synchronous, oscillations for the same network parameters. This is different from the reverberating activity studied earlier, where the two states were silence and fast oscillations.

7.1 A Network Memory Effect. With random, sparse connectivity, there is a significant parameter range in which there is a finite but fairly large number of population spike volleys before the network comes to rest (see Figure 12A). In our earlier models, an action potential has the effect

that the membrane potential and the synaptic gating variables are reset, and thereby the past is forgotten. What happens after the second action potential is precisely what happened after the first. Therefore, if there is a second action potential, there will be infinitely many. The network in Figure 12A fires seven spike volleys following the initial stimulation period and then comes to rest. How does it "remember" its past? What makes the seventh spike volley different from the first? The answer is that the number of E-cells participating in the spike volleys slowly decreases with time. Each time this number decreases, the recurrent excitation generated by the E-cell spike volley also decreases, and therefore on the next cycle, even fewer E-cells participate and there is even less recurrent excitation, and so on. In fact, the numbers of participating E-cells in the seven spike volleys in Figure 12A are 84, 87, 83, 81, 75, 71, and 48. That the number of participating cells is slightly greater on the second volley than on the first is the result of residual recurrent excitation from the initial 100 ms period of high-frequency random stimulation, in addition to the strong recurrent excitation generated by the first volley. This discussion also explains the gradual slowing of the rhythm in Figure 12A.

7.2 Coexistence of Slow and Fast Oscillations. With parameters precisely as in Figure 11B, it is possible to maintain slow firing (see Figure 12B). The E- and I-cells are initialized synchronously in Figure 12B but not in Figure 11B. Two different positive frequencies are possible for the same network parameters, depending on whether the E-cells are more (in Figure 12B) or less (in Figure 11B) synchronous.

8 Discussion

In this letter, we have focused on the mathematical analysis of the simplest possible models of rhythmic reverberating activity and runaway transitions based on recurrent excitation. We believe that this is useful and important. Of course, we have omitted many important aspects of real neuronal networks, some of which we discuss here.

Our modeling has been kept as simple as possible deliberately. In particular, we have assumed the rise of the synaptic gating variable following an action potential to be instantaneous in all cases, except for the network model described in the appendix. More realistic synaptic models with positive rise times (differences of exponentials for instance) could be used in the analysis. In fact, while preparing this letter, we did study the self-exciting theta neuron with a synaptic gating variable with positive rise time; we are not presenting these results here because they are not significantly different from those for an instantaneously rising synaptic gating variable. In addition, the network simulations, in which the synaptic gating variables do have positive rise times, yield results that to a large extent (although, of course, not completely) match those suggested by the single-cell models,

strengthening our confidence that the assumption of instantaneously rising gating variables is not essential here.

Another important feature of real neuronal dynamics that we have omitted is refractoriness. Of course, the Hodgkin-Huxley–like models defined in the appendix do have refractoriness built in implicitly. Immediately following an action potential, input is ineffective because the gating variables of the ionic currents are still large. Even the theta neuron has some built-in refractoriness in the sense that input that comes immediately after an action potential is relatively ineffective (see, e.g., Figure 25.11 of Börgers, 2017). In the LIF models that we study here, refractoriness could be built in explicitly. Following an action potential, we could assume that v remains at 0 for some short time period τ_{ref}, for instance. However, this would simply amount to weakening the excitatory and inhibitory autapses by factors of $e^{-\tau_{\text{ref}}/\tau_e}$ and $e^{-\tau_{\text{ref}}/\tau_i}$, respectively, and adding τ_{ref} to the firing period, which would have simple and predictable consequences for the f-I-g_e surfaces and would in particular not change our conclusions qualitatively. Refractoriness certainly prevents runaway *activity* in the sense of extremely high frequencies, since a neuron with a refractory period of τ_{ref} cannot fire with a period shorter than τ_{ref}. Our focus here has been on runaway *transitions*, which we define to be jump discontinuities in the dependence of frequency on parameters.

We have focused on reverberating activity that is rhythmic. Rhythmic reverberating activity is of interest because there is experimental evidence that rhythmicity plays a role in working memory (Alekseichuk et al., 2016; Leszczyński et al., 2015; Roux & Uhlhaas, 2014; Yamamoto et al., 2014). However, asynchronous reverberating activity is certainly possible in models (Gutkin et al., 2001; Wang, 1999), and in fact synchrony can be the mechanism that terminates reverberating activity driven by rapidly decaying recurrent excitation (Gutkin et al., 2001).

Several authors have pointed out that reverberating firing driven by recurrent excitation is not the only possible working memory mechanism. An overview of possible mechanisms can be found in Barak and Tsodyks (2014). For example, bistability of individual cells may also allow persistent activity (Camperi & Wang, 1998), and transient facilitation of recurrent synaptic connections was suggested in Mongillo et al. (2008) and Barak and Tsodyks (2007) as a mechanism that may be important for working memory (see also Hansel & Mato, 2013). In the modeling study of Papoutsi, Sidiropoulou, Cutsuridis, & Poirazi (2013), the potential role of modulation of h-currents, AHP currents, D-type potassium currents, and calcium currents is explored.

Firing of pyramidal cells in prefrontal cortex during working memory tasks has been reported to be highly irregular (Compte et al., 2003; Shinomoto, Sakai, & Funahashi, 1999). This is not necessarily incompatible with rhythmic population activity, since individual cells may not participate on all cycles of a rhythm (for modeling studies of such rhythms see, e.g., Börgers, Epstein, & Kopell, 2005; Kilpatrick & Ermentrout, 2011; Kopell &

LeMasson, 1994; Krupa, Gielen, & Gutkin, 2014; and Traub et al., 2000). Although we have focused here on rhythms in which all cells fire on each population cycle, at least some of the conclusions reached here appear to hold for rhythms in which participation of individual cells is irregular (Takeuchi, 2017).

The coexistence of seizure activity (very fast firing) with slower firing, numerically observed in section 7.2, was found and analyzed in a very different model in Lee, Ermentrout, and Bodner (2013). They emphasized changing the strength of feedback inhibition. By contrast, we have taken the strength of feedback inhibition to be fixed and varied the strengths of recurrent and external excitation. An increase in the strength of feedback inhibition would move both the onset edge of reverberating activity and any runaway transition to larger values of g_e.

We have studied how the combination of fast recurrent excitation with slow feedback inhibition can result in discontinuous dependence of frequency on parameter values. We note that the role of the feedback inhibition could also be played by a long-lasting adaptation current; at the level of our single-cell models, such a current is not even distinguishable from feedback inhibition. Subthreshold currents, such as h- and persistent sodium currents, can play a crucial role in determining where the runaway transitions occur (Rotstein, 2013; Schindewolf, Kim, Bel, & Rotstein, 2016).

A number of authors have argued that the balance of excitatory and inhibitory synaptic inputs in the cortex is the key to preventing runaway activity (Tsodyks, Skaggs, Sejnowski, & McNaughton, 1997; Vogels, Rajan, & Abbott, 2005). Our result is not in contradiction with this idea, and in particular does not rule out the possibility that greater recurrent excitation recruits more feedback inhibition, thereby preventing or delaying a runaway transition. We have only studied what happens when the feedback inhibition strength is fixed while recurrent and external excitation are varied.

We conclude with a brief summary and discussion of our three main results:

- Reverberating activity can be fueled by extremely weak, slow recurrent excitation, but only by sufficiently strong, fast recurrent excitation. We note that this is by no means obvious: Fast recurrent excitation could, one might think, produce recurrent excitation even if it is weak, as long as the neurons in the network are sufficiently close to the firing threshold already because of external drive. We show that at least in our models, this is not so.
- The onset of reverberating activity, as recurrent excitation is strengthened or external drive is raised, occurs at a positive frequency. It is slower when the recurrent excitation has a longer decay time constant. It is faster when the external drive is weaker (and the recurrent excitation stronger). As we have pointed out, this implies that compensating for the loss of one kind of excitatory drive

Table 1: Physical Units Used throughout This Letter.

Quantity	Typical Letters	Unit
Voltage	v	mV
Time	t, τ, T	ms
Frequency	f	$\text{Hz} = \text{s}^{-1}$
Current density	I	$\mu\text{A/cm}^2$
Conductance density	g	mS/cm^2
Capacitance density	C	$\mu\text{F/cm}^2$

(recurrent synaptic excitation) with another (external drive) can restore rhythmic reverberating activity at a different population frequency.

- Runaway transitions only occur with fast, not slow, recurrent excitation. Runaway transitions arise in the following kind of situation. Recurrent excitation resulting from a population spike volley is initially strong enough to reactivate the neurons of the network after a short time but is prevented from doing so by a burst of feedback inhibition. By the time the feedback inhibition disappears, the recurrent excitation is too weak to reactivate the population immediately, and it is only re-activated much later, for instance, because of external drive. It is clear that in such a situation, a slight increase in recurrent excitation strength or a slight decrease in the strength of feedback inhibition can abruptly tip the balance, permitting rapid activity driven by recurrent excitation. It is not obvious, but shown by our analysis and confirmed by our network simulations, that this requires the recurrent excitation to decay more rapidly than the feedback inhibition regardless of how large the maximal synaptic conductances are.

We have also demonstrated that the relation between reverberating activity fueled by recurrent excitation and runaway transitions can be visualized in an instructive way by a (generalized) cusp catastrophe surface.

Appendix: Biophysical E-I Network Model

A.1 Physical Units. We usually omit units, but we always mean the units in Table 1. Because the period T of a periodically firing neuron is taken to be measured in ms, but its frequency f is measured not in ms^{-1} but in $\text{s}^{-1} = \text{Hz}$, the relation between f and T is $f = 1000/T$.

A.2 E-Cells. The model that we use here is a slight modification of a model due to Ermentrout and Kopell (1998), which in turn is a reduction of a model of a pyramidal excitatory cell in rat hippocampus due to Traub and Miles (1991). The equations are of the form of the classical Hodgkin-Huxley

model, with the simplifying assumption of infinitely fast sodium activation:

$$C\frac{dv}{dt} = \bar{g}_{\mathrm{Na}}\,(m_\infty(v))^3\,h(v_{\mathrm{Na}} - v) + \bar{g}_{\mathrm{K}}n^4(v_{\mathrm{K}} - v) + \bar{g}_{\mathrm{L}}(v_{\mathrm{L}} - v) + I, \quad \text{(A.1)}$$

$$\frac{dx}{dt} = \alpha_x(v)(1 - x) - \beta_x(v)x, \;\; x = h, n. \quad \text{(A.2)}$$

Using the units specified in Table 1,

$$C = 1, v_{\mathrm{Na}} = 50, v_{\mathrm{K}} = -100, v_{\mathrm{L}} = -67, \bar{g}_{\mathrm{Na}} = 100, \bar{g}_{\mathrm{K}} = 80, \bar{g}_{\mathrm{L}} = 0.1.$$

Furthermore,

$$\begin{aligned}
m_\infty(v) &= \frac{\alpha_m(v)}{\alpha_m(v) + \beta_m(v)},\\
\alpha_m(v) &= \frac{0.32(v + 54)}{1 - \exp(-(v + 54)/4)}, \quad \beta_m(v) = \frac{0.28(v + 27)}{\exp((v + 27)/5) - 1},\\
\alpha_h(v) &= 0.128\exp(-(v + 50)/18), \quad \beta_h(v) = \frac{4}{1 + \exp(-(v + 27)/5)},\\
\alpha_n(v) &= \frac{0.032(v + 52)}{1 - \exp(-(v + 52)/5))}, \quad \beta_n(v) = 0.5\exp(-(v + 57)/40).
\end{aligned} \quad \text{(A.3)}$$

The model neuron fires periodically if and only if $I > I_c$, with

$$I \approx 0.12$$

(see section 17.2 of Börgers, 2017).

A.3 I-Cells. For the I-cells, we use the model of inhibitory basket cells in rat hippocampus introduced by Wang and Buzsáki (1996). (This model included a scaling factor ϕ in front of the formulas for α_h, β_h, α_n, and β_n. The authors chose $\phi = 5$. This choice is built into the equations as stated below.) The model is given by equations A.1 to A.3, with

$$\begin{aligned}
C = 1, v_{\mathrm{Na}} = 55, v_{\mathrm{K}} = -90, v_{\mathrm{L}} = -65, \bar{g}_{\mathrm{Na}} = 35, \bar{g}_{\mathrm{K}} = 9, \bar{g}_{\mathrm{L}} = 0.1,\\
\alpha_m(v) = \frac{0.1(v + 35)}{1 - \exp(-(v + 35)/10))}, \beta_m(v) = 4\exp(-(v + 60)/18),\\
\alpha_h(v) = 0.35\exp(-(v + 58)/20), \beta_h(v) = \frac{5}{1 + \exp(-0.1(v + 28))},
\end{aligned}$$

$$\alpha_n(v) = \frac{0.05(v+34)}{1-\exp(-0.1(v+34))}, \beta_n(v) = 0.625\exp(-(v+44)/80).$$

The model neuron fires periodically if and only if $I > I_c$, with

$$I \approx 0.16$$

(see Figure 17.7 of Börgers, 2017).

A.4 Synapses. In model networks, we associate with each synapse a gating variable s varying between 0 and 1, governed by a differential equation of the form

$$\frac{ds}{dt} = \frac{1+\tanh(v/10)}{2}\frac{1-s}{0.1} - \frac{s}{\tau_d}, \tag{A.4}$$

where $\tau_d = 3$ for E-to-I synapses and $\tau_d = 10$ for inhibitory synapses. We write

$$\tau_e = \text{value of } \tau_d \text{ for E-to-E synapses.}$$

This value will be varied. We do not include a model of the magnesium block of NMDA receptors in this letter (see Takeuchi, 2017, for numerical experiments including this effect).

The activity of a cell with synaptic gating variable s gives rise to synaptic currents into postsynaptic cells. If the membrane potential of a postsynaptic cell is v_{post}, the synaptic current is of the form

$$I_{\text{syn}} = \bar{g}_{\text{syn}} s(t)(v_{\text{rev}} - v_{\text{post}}),$$

where $\bar{g}_{\text{syn}} \geq 0$ is a fixed maximal conductance and v_{rev} is the synaptic reversal potential.

A.5 E-I Networks. We consider networks of N_e E-cells and N_i I-cells, with $N_e = 100$ and $N_i = 25$. The I-cells receive zero external drive. We assume here for simplicity that all E-cells receive the same external drive and write

$$I = \text{drive to the E-cells.}$$

Omitting heterogeneity in external drives has the effect that we can say without ambiguity whether the external drive is above or below threshold. Heterogeneity effects do play a role in one of our network simulations in

this letter; the kind of heterogeneity included here comes from variability in the numbers of synaptic inputs per cell.

For any pair of neurons in the network, we define parameters associated with a synapse from one neuron into the other (compare section A.4):

$$\bar{g}_{\text{syn}}, v_{\text{rev}}, \tau_d.$$

To set the strengths (maximal conductances) of the synaptic connections from E-cells to I-cells, we choose two parameters, $\hat{g}_{ei} \geq 0$ and $p_{ei} \in (0, 1]$. The maximal conductance associated with the ith E-cell and the jth I-cell is then

$$\bar{g}_{\text{syn},ei,ij} = \frac{\hat{g}_{ei} Z_{ei,ij}}{p_{ei} N_e}, \tag{A.5}$$

where the $Z_{ei,ij}$ are independent random numbers with

$$Z_{ei,ij} = \begin{cases} 1 \text{ with probability } p_{ei}, \\ 0 \text{ otherwise.} \end{cases}$$

Note that $\hat{g}_{ei}$ is the expected total amount of excitatory conductance affecting an I-cell:

$$E\left(\sum_{i=1}^{N_e} \bar{g}_{\text{syn},ei,ij}\right) = \hat{g}_{ei}.$$

The strengths of the I-to-E, E-to-E, and I-to-I synapses are set similarly. We write

$$g_e = \hat{g}_{ee}.$$

The reversal potentials v_{rev} are always taken to be 0 for excitatory synapses and -75 for inhibitory synapses.

A.6 High-Frequency Stochastic Input. In several of our network simulations, we generate high-frequency asynchronous activity in the E-cells during the initial 100 ms by adding to the right-hand side of the equation governing the membrane potential, v_i, of the ith E-cell a term of the form

$$-0.25 s_{\text{stoch},i}(t) v_i.$$

At the end of each time step of the numerical simulation, the function $s_{\text{stoch},i}$ jumps to 1 with probability

$$\frac{f_{\text{stoch}}\Delta t}{1000},$$

with $f_{\text{stoch}} > 0$. The times of jumps in $s_{\text{stoch},i}$ for different i are independent of each other. Between jumps, $s_{\text{stoch},i}$ decays exponentially with decay time constant τ_{stoch}. This is a crude model of bombardment by excitatory synaptic inputs arriving at random times with mean frequency f_{stoch} (measured in Hz). We always use $f_{\text{stoch}} = 40$ in this letter. We choose a decay time constant τ_{stoch} comparable to that of AMPA-receptor-mediated synaptic currents: $\tau_{\text{stoch}} = 3$ ms.

Acknowledgments

C. B. and R. M. T. were supported in part through the Collaborative Research in Computational Neuroscience program by NIH grant 1R01 NS067199.

References

Alekseichuk, I., Turi, Z., de Lara, G. A., Antal, A., & Paulus, W. (2016). Spatial working memory in humans depends on theta and high gamma synchronization in the prefrontal cortex. *Current Biology*, *26*(12), 1513–1521.

Barak, O., & Tsodyks, M. (2007). Persistent activity in neural networks with dynamic synapses. *PLoS Comp. Biol.*, *3*(2), e35.

Barak, O., & Tsodyks, M. (2014). Working models of working memory. *Current Opinion in Neurobiology*, *25*, 20–24.

Börgers, C. (2017). *An introduction to modeling neuronal dynamics*. New York: Springer.

Börgers, C., Epstein, S., & Kopell, N. (2005). Background gamma rhythmicity and attention in cortical local circuits: A computational study. *Proc. Natl. Acad. Sci. USA*, *102*(19), 7002–7007.

Börgers, C., & Kopell, N. (2005). Effects of noisy drive on rhythms in networks of excitatory and inhibitory neurons. *Neural Comput.*, *17*(3), 557–608.

Buzsáki, G., & Wang, X.-J. (2012). Mechanisms of gamma oscillations. *Annu. Rev. Neurosci.*, *35*(1), 203–225.

Camperi, M., & Wang, X.-J. (1998). A model of visuospatial working memory in prefrontal cortex: Recurrent network and cellular bistability. *J. Comp. Neurosci.*, *5*(4), 383–405.

Compte, A., Brunel, N., Goldman-Rakic, P. S., & Wang, X.-J. (2000). Synaptic mechanisms and network dynamics underlying spatial working memory in a cortical network model. *Cerebral Cortex*, *10*(9), 910–923.

Compte, A., Constantinidis, C., Tegner, J., Raghavachari, S., Chafee, M. V., Goldman-Rakic, P. S., & Wang, X.-J. (2003). Temporally irregular mnemonic persistent activity in prefrontal neurons of monkeys during a delayed response task. *J. Neurophysiol.*, *90*(5), 3441–3454.

Coyle, J. T. (2012). NMDA receptor and schizophrenia: A brief history. *Schizophrenia Bulletin*, *38*(5), 920–926.

Eichhammer, P., Wiegand, R., Kharraz, A., Langguth, B., Binder, H., & Hajak, G. (2004). Cortical excitability in neuroleptic-naive first-episode schizophrenic patients. *Schizophrenia Research*, *67*(2–3), 253–259.

Ermentrout, B. (2008). Ermentrout-Kopell canonical model. *Scholarpedia*, *3*(3), 1398.

Ermentrout, G. B., & Kopell, N. (1986). Parabolic bursting in an excitable system coupled with a slow oscillation. *SIAM J. Appl. Math*, *46*, 233–253.

Ermentrout, G. B., & Kopell, N. (1998). Fine structure of neural spiking and synchronization in the presence of conduction delay. *Proc. Natl. Acad. Sci. USA*, *95*, 1259–1264.

Faulkner, M. A., & Burke, R. A. (2013). Safety profile of two novel antiepileptic agents approved for the treatment of refractory partial seizures: Ezogabine (retigabine) and perampanel. *Expert Opinion on Drug Safety*, *12*(6), 847–855.

Gerstner, W., van Hemmen, J. L., & Cowan, J. D. (1996). What matters in neuronal locking? *Neural Comput.*, *8*(8), 1653–1676.

Goldman-Rakic, P. S. (1994). Working memory dysfunction in schizophrenia. *J. Neuropsychiatry Clin. Neurosci.*, *6*(4), 348–357.

Gómez, L., Budelli, R., & Pakdaman, K. (2001). Dynamical behavior of a pacemaker neuron model with fixed delay stimulation. *Phys. Rev. E*, *64*, 061910.

Gutkin, B. S., Laing, C. R., Colby, C. L., Chow, C. C., & Ermentrout, G. B. (2001). Turning on and off with excitation: The role of spike-timing asynchrony and synchrony in sustained neural activity. *J. Comp. Neurosci.*, *11*, 121–134.

Hansel, D., & Mato, G. (2013). Short-term plasticity explains irregular persistent activity in working memory tasks. *J. Neurosci.*, *33*(1), 133–149.

Kilpatrick, Z. P., & Ermentrout, G. B. (2011). Sparse gamma rhythms arising through clustering in adapting neuronal networks. *PLoS Comput. Biol.*, *7*(11), e1002281.

Kopell, N., & LeMasson, G. (1994). Rhythmogenesis, amplitude modulation, and multiplexing in a cortical architecture. *Proc. Natl. Acad. Sci. USA*, *91*(22), 10586–10590.

Krupa, M., Gielen, S., & Gutkin, B. (2014). Adaptation and shunting inhibition leads to pyramidal/interneuron gamma with sparse firing of pyramidal cells. *J. Comp. Neurosci.*, *37*(2), 357–376.

Lee, J., Ermentrout, B., & Bodner, M. (2013). From cognitive networks to seizures: Stimulus evoked dynamics in a coupled cortical network. *Chaos*, *23*(4), 043111.

Leszczyński, M., Fell, J., & Axmacher, N. (2015). Rhythmic working memory activation in the human hippocampus. *Cell Reports*, *13*(6), 1272–1282.

Li, N., Daie, K., Svoboda, K., & Druckmann, S. (2016). Robust neuronal dynamics in premotor cortex during motor planning. *Nature*, *532*(7600), 459–464.

McCormick, D. A., & Contreras, D. (2001). On the cellular and network bases of epileptic seizures. *Annu. Rev. Physiol.*, *63*, 815–846.

McCormick, D. A., Hasenstaub, Y. S. A., Sanchez-Vives, M., Badoual, M., & Bal, T. (2003). Persistent cortical activity: Mechanisms of generation and effects on neuronal excitability. *Cerebral Cortex*, *13*(11), 1219–1231.

Mirollo, R. E., & Strogatz, S. H. (1990). Synchronization of pulse-coupled biological oscillators. *SIAM J. Appl. Math.*, *50*, 1645–1662.

Mongillo, G., Barak, O., & Tsodyks, M. (2008). Synaptic theory of working memory. *Science*, *319*(5869), 1543–1546.

Mormann, F., & Jefferys, J. G. R. (2013). Neuronal firing in human epileptic cortex: The ins and outs of synchrony during seizures. *Epilepsy Curr.*, *13*, 100–102.

Papoutsi, A., Sidiropoulou, K., Cutsuridis, V., & Poirazi, P. (2013). Induction and modulation of persistent activity in a layer V PFC microcircuit model. *Frontiers in Neural Circuits*, *7*, 161.

Peskin, C. S. (1975). *Mathematical aspects of heart physiology*. New York: Courant Institute of Mathematical Sciences, New York University.

Riley, M. R., & Constantinidis, C. (2015). Role of prefrontal persistent activity in working memory. *Frontiers in Systems Neuroscience*, *9*, 181.

Rogawski, M. A. (2013). AMPA receptors as a molecular target in epilepsy therapy. *Acta Neurologica Scandinavica*, *127*, 9–18.

Rotstein, H. G. (2013). Abrupt and gradual transitions between low and hyperexcited firing frequencies in neuronal models with fast synaptic excitation: A comparative study. *Chaos*, *23*(4), 046104.

Roux, F., & Uhlhaas, P. J. (2014). Working memory and neural oscillations: α-γ versus θ-γ codes for distinct WM information? *Trends in Cognitive Sciences*, *18*(1), 16–25.

Schindewolf, C., Kim, D., Bel, A., & Rotstein, H. G. (2016). Complex patterns in networks of hyperexcitable neurons. *Theoretical Computer Science*, *633*, 71–82.

Seung, H. S., Lee, D. D., Reis, B. Y., & Tank, D. W. (2000). The autapse: A simple illustration of short-term analog memory storage by tuned synaptic feedback. *J. Comput. Neurosci.*, *9*(2), 171–185.

Shinomoto, S., Sakai, Y., & Funahashi, S. (1999). The Ornstein-Uhlenbeck process does not reproduce spiking statistics of neurons in prefrontal cortex. *Neural Comput.*, *11*(4), 935–951.

Spencer, K. M., Nestor, P. G., Perlmutter, R., Niznikiewicz, M. A., Klump, M. C., Frumin, M., . . . McCarley, R. W. (2004). Neural synchrony indexes disordered perception and cognition in schizophrenia. *Proc. Natl. Acad. Sci. USA*, *101*(49), 17288–17293.

Strogatz, S. H. (2015). *Nonlinear dynamics and chaos* (2nd ed.). Boulder, CO: Westview Press.

Takeuchi, R. M. (2017). *An analysis of neuronal networks with recurrent excitation*. PhD dissertation, Tufts University.

Tiesinga, P., & Sejnowski, T. J. (2009). Cortical enlightenment: Are attentional gamma oscillations driven by ING or PING? *Neuron*, *63*(6), 727–732.

Traub, R. D., Bibbig, A., Fisahn, A., LeBeau, F. E. N., Whittington, M. A., & Buhl, E. H. (2000). A model of gamma-frequency network oscillations induced in the rat CA3 region by carbachol in vitro. *Eur. J. Neurosci.*, *12*, 4093–4106.

Traub, R. D., & Miles, R. (1991). *Neuronal networks of the hippocampus*. Cambridge: Cambridge University Press.

Tsodyks, M. V., Skaggs, W. E., Sejnowski, T. J., & McNaughton, B. L. (1997). Paradoxical effects of external modulation of inhibitory interneurons. *J. Neurosci.*, *17*(11), 4382–4388.

Vogels, T. P., Rajan, K., & Abbott, L. F. (2005). Neural network dynamics. *Annu. Rev. Neurosci.*, *28*(1), 357–376.

Wang, M., & Arnsten, A. F. T. (2015). Contribution of NMDA receptors to dorsolateral prefrontal cortical networks in primates. *Neuroscience Bulletin*, *31*(2), 191–197.

Wang, M., Yang, Y., Wang, C.-J., Gamo, N. J., Jin, L. E., Mazer, J. A., . . . and Arnsten, A. F. T. (2013). NMDA receptors subserve persistent neuronal firing during working memory in dorsolateral prefrontal cortex. *Neuron*, *77*(4), 736–749.

Wang, X. J. (1999). Synaptic basis of cortical persistent activity: The importance of NMDA receptors to working memory. *J. Neurosci.*, *19*(21), 9587–9603.

Wang, X.-J., & Buzsáki, G. (1996). Gamma oscillation by synaptic inhibition in a hippocampal interneuronal network model. *J. Neurosci.*, *16*, 6402–6413.

Whittington, M. A., Traub, R. D., Kopell, N., Ermentrout, B., & Buhl, E. H. (2000). Inhibition-based rhythms: Experimental and mathematical observations on network dynamics. *Int. J. Psychophysiol.*, *38*, 315–336.

Xie, X., & Seung, H. S. (2000). Spike-based learning rules and stabilization of persistent neural activity. In S. A. Solla, T. K. Leen, & K. Müller (Eds.), *Advances in neural information processing systems, 12* (pp. 199–208). Cambridge, MA: MIT Press.

Yamamoto, J., Suh, J., Takeuchi, D., & Tonegawa, S. (2014). Successful execution of working memory linked to synchronized high-frequency gamma oscillations. *Cell*, *157*(4), 845–857.

Zwart, R., Sher, E., Ping, X., Jin, X., Sims, J. R., Chappell, A. S., . . . Witkin, J. M. (2014). Perampanel, an antagonist of amino-3-hydroxy-5-methyl-4-isoxazolepropionic acid receptors, for the treatment of epilepsy: Studies in human epileptic brain and nonepileptic brain and in rodent models. *J. Pharmacol. Exp. Ther.*, *351*(1), 124–133.

Received April 17, 2017; accepted August 22, 2017.